HHS Public Access

Author manuscript

Nature. Author manuscript; available in PMC 2025 February 07.

Published in final edited form as:

Nature. 2024 February ; 626(7999): 626–634. doi:10.1038/s41586-024-07018-7.

Naturally occurring T cell mutations enhance engineered T cell therapies

Julie Garcia[1,2,14,15], **Jay Daniels**[1,3,4,14,15], **Yujin Lee**[3,4], **Iowis Zhu**[1,2], **Kathleen Cheng**[3,4], **Qing Liu**[3,4], **Daniel Goodman**[1,2], **Cassandra Burnett**[1,2], **Calvin Law**[3,4], **Chloë Thienpont**[1], **Josef Alavi**[1], **Camillia Azimi**[1,2], **Garrett Montgomery**[1], **Kole T. Roybal**[1,2,5,6,7,8,9,✉], **Jaehyuk Choi**[3,4,10,11,12,13,✉]

[1]Department of Microbiology and Immunology, University of California, San Francisco, San Francisco, CA, USA.

[2]Parker Institute for Cancer Immunotherapy, San Francisco, CA, USA.

[3]Department of Dermatology, Northwestern University Feinberg School of Medicine, Chicago, IL, USA.

[4]Department of Biochemistry and Molecular Genetics, Northwestern University Feinberg School of Medicine, Chicago, IL, USA.

[5]Chan Zuckerberg Biohub, San Francisco, CA, USA.

[6]Helen Diller Family Comprehensive Cancer Center, University of California, San Francisco, San Francisco, CA, USA.

[7]Department of Anesthesia, University of California, San Francisco, San Francisco, CA, USA.

[8]Gladstone-UCSF Institute for Genomic Immunology, San Francisco, CA, USA.

[9]UCSF Cell Design Institute, San Francisco, CA, USA.

✉**Correspondence and requests for materials** should be addressed to Kole T. Roybal or Jaehyuk Choi. kole.roybal@ucsf.edu; jaehyuk.choi@northwestern.edu.

Author contributions J.G., J.D., K.T.R. and J.C. designed the study. J.G. carried out in vivo screening, primary T cell in vitro experiments and in vivo CAR T cell experiments. J.D. carried out in vitro screening, biochemical experiments, in vivo TCR-transgenic experiments and bioinformatics analysis. J.D. and J.C. identified library mutations. J.G., I.Z. and D.G. designed the lentiviral library; J.G. and I.Z. cloned the library. J.G. produced the lentivirus of each construct. C.T., C.B., J.A. and C.A assisted with in vivo CAR T cell experiments. Y.L., Q.L., K.C. and C.L. assisted with biochemical and in vivo TCR-transgenic experiments. K.C., Q.L. and C.L. carried out and analysed the necropsies. G.M. assisted with primary T cell isolations from human donors. J.G., J.D., K.T.R. and J.C. wrote the manuscript with input from all authors. K.T.R. and J.C. supervised the study.

Online content

Any methods, additional references, Nature Portfolio reporting summaries, source data, extended data, supplementary information, acknowledgements, peer review information; details of author contributions and competing interests; and statements of data and code availability are available at https://doi.org/10.1038/s41586-024-07018-7.

Reporting summary

Further information on research design is available in the Nature Portfolio Reporting Summary linked to this article.

Competing interests K.T.R. is a co-founder, consultant, SAB member and stockholder of Arsenal Biosciences and Dispatch Therapeutics. He was a founding scientist and consultant and stockholder in Cell Design Labs, now a Gilead Company. K.T.R. holds stock in Gilead. K.T.R. is an exclusive adviser to Venrock. J.G. and J.D. are founding scientists and stockholders of Moonlight Bio. K.T.R. and J.C. are co-founders and stockholders of Moonlight Bio. K.T.R., J.C., J.G., J.D. and I.Z. are inventors on a University of California, San Francisco and Northwestern University provisional patent for enhancing adoptive T cell therapeutics; 63/412,300.

Supplementary information The online version contains supplementary material available at https://doi.org/10.1038/s41586-024-07018-7.

[10]Center for Synthetic Biology, Northwestern University, Evanston, IL, USA.

[11]Center for Human Immunobiology, Northwestern University Feinberg School of Medicine, Chicago, IL, USA.

[12]Center for Genetic Medicine, Northwestern University Feinberg School of Medicine, Chicago, IL, USA.

[13]Robert H. Lurie Comprehensive Cancer Center, Northwestern University Feinberg School of Medicine, Chicago, IL, USA.

[14]Present address: Moonlight Bio, Seattle, WA, USA.

[15]These authors contributed equally: Julie Garcia, Jay Daniels.

Abstract

Adoptive T cell therapies have produced exceptional responses in a subset of patients with cancer. However, therapeutic efficacy can be hindered by poor T cell persistence and function[1]. In human T cell cancers, evolution of the disease positively selects for mutations that improve fitness of T cells in challenging situations analogous to those faced by therapeutic T cells. Therefore, we reasoned that these mutations could be co-opted to improve T cell therapies. Here we systematically screened the effects of 71 mutations from T cell neoplasms on T cell signalling, cytokine production and in vivo persistence in tumours. We identify a gene fusion, *CARD11–PIK3R3*, found in a $CD4^+$ cutaneous T cell lymphoma[2], that augments CARD11–BCL10–MALT1 complex signalling and anti-tumour efficacy of therapeutic T cells in several immunotherapy-refractory models in an antigen-dependent manner. Underscoring its potential to be deployed safely, CARD11–PIK3R3-expressing cells were followed up to 418 days after T cell transfer in vivo without evidence of malignant transformation. Collectively, our results indicate that exploiting naturally occurring mutations represents a promising approach to explore the extremes of T cell biology and discover how solutions derived from evolution of malignant T cells can improve a broad range of T cell therapies.

T cell therapies have revolutionized cancer therapy for haematological cancers but have not yet been consistently effective in solid tumours, which represent 90% of adult cancers[3]. In both solid tumours and treatment-resistant haematological malignancies, they are limited by a combination of factors, including poor in vivo persistence, immunosuppressive environmental factors and T cell exhaustion[4].

To address these shortcomings, we turned to T cell neoplasms, which include both clonal T cells in autoinflammatory syndromes[5,6] and T cell lymphomas[7–9]. They acquire mutations that increase their fitness and enable positive selection in a solid tumour-like immunosuppressive microenvironment. This approach takes advantage of evolution that uses any mutation available in nature, which can have unique, outsized effects unachievable by modulation of wild-type gene expression. Underscoring the value of this approach, many potency enhancements that improve T cell therapies in preclinical models (for example, inactivation of *PDCD1*, *TET2* or *DNMT3A*) have already been identified as mutations in T cell lymphomas[8,10–12].

Here we have generated a library of 71 mutations and 45 wild-type controls. We introduce these mutations into human and mouse T cells and assess their effects on T cell phenotypes in vitro and in vivo using arrayed and pooled screens. Through these efforts, we have identified a fusion of caspase recruitment domain-containing protein 11 (CARD11) and phosphoinositide-3-kinase regulatory subunit 3 (PIK3R3) that markedly increases AP-1 and NF-κB signalling, interleukin-2 (IL-2) production and tumour killing in vitro and in vivo. CARD11–PIK3R3 improves chimeric antigen receptor (CAR) and T cell receptor (TCR) T cell anti-tumour activity, reduces T cell dose requirements and relieves the requirement for harsh lymphodepletion preconditioning.

In vitro and in vivo mutation screening

First, we identified 71 mutations in putative drivers of clonal T cell neoplasms[7–9] (Supplementary Table 1). These included 61 point mutations (encoding non-synonymous amino acid substitutions and putative gain-of-function truncating mutations) in 40 different genes. For each point mutation, there was a wild-type control. In addition, we cloned ten gene fusions and five controls (Fig. 1a). These genes were cloned into a bar-coded lentiviral construct to enable pooled screening, altogether creating a library of 116 unique constructs.

To elucidate the effects of these mutations on T cell phenotypes, we generated a triple-reporter Jurkat cell line for NFAT, NF-κB and AP-1 pathway activation. These reporter cells were transduced with either a CD19-CD28z-CAR or a CD19-BBz-CAR (Extended Data Fig. 1a), and a construct in the library. At 24-h post co-culture with $CD19^+$ or $CD19^-$ target cell lines (Extended Data Fig. 1a), activation of the three T cell signalling pathways was measured by flow cytometry (Extended Data Fig. 1b,c). IL-2 production was assessed by enzyme-linked immunosorbent assay (ELISA). For the CD19-BBz-CAR screen, levels of PD1 (also known as PDCD1) were also assessed.

This screen uncovered numerous mutations with a notable impact on CAR signalling and phenotypes (Fig. 1b and Extended Data Fig. 1d). These screens were reproducible across experimental replicates and in both CD28z-CAR and BBz-CAR screens (Extended Data Fig. 1e–g). To identify patterns, we carried out unbiased *k*-means clustering (Fig. 1b). Gain-of-function mutations in the same genes (for example, *PLCG1* and *CARD11*) tended to cluster together and activate or inhibit similar pathways to varying extents. The mutations produced strikingly diverse effects on TCR-dependent signalling and T cell phenotypes (Fig. 1c–e). For the BBz-CAR, ten different combinations of signalling pathway upregulation or downregulation induced by mutations were observed, providing a toolkit of modifications that could be used to influence signalling, such as to combat imbalances between NFAT and AP-1 signalling that may contribute to T cell exhaustion[13].

A total of 24 point mutations had significant differences in signalling compared to wild-type controls (Extended Data Fig. 2a–c). For example, AP-1 reporter expression could be tuned down by 60% or increased to nearly threefold (Fig. 1d). These effects are more pro-found in IL-2 production, with nine mutations driving higher levels of IL-2 than attained with any wild-type gene tested (Fig. 1e). Although mutations in the same gene tend to have similar qualitative effects, the effect size can vary widely. For example, IL-2 increased 15-

to 396-fold among *BRAF* mutations and 114- to 359-fold for *CARD11* mutations (Fig. 1e). Our previous work[7] suggested that some mutations require antigen stimulation to exert their effects. Particularly for the BBz-CAR, the mutations had significantly less effects without antigen compared to with antigen (Extended Data Fig. 2d). Collectively, this T cell mutation library provides a powerful and tunable toolkit for rewiring the balance and strength of different T cell signalling pathways and functional outputs in response to CAR signalling.

A major barrier to successful cell therapy is the accumulation and persistence of T cells within tumours[3]. As these mutations were positively selected in patients, we reasoned that they could improve in vivo persistence of human CAR T cells. Therefore, we systematically screened mutations in primary human CAR T cells in a xenograft model. We used a fast-growing K562 subcutaneous tumour model in which CAR T cell efficacy is limited (Extended Data Fig. 3a). To screen mutations in vivo, primary human T cells were individually co-transduced with a CD19-BBz-CAR and the mutation constructs. They were then pooled, sorted and injected into immunodeficient mice bearing subcutaneous CD19-K562 tumours. A sample of this pre-injection pooled library was taken for baseline sequencing of bar-codes (Extended Data Fig. 3b). Bar-code frequency in tumours was compared to the pre-injection T cell pool to determine constructs that were depleted or enriched in vivo. Reassuringly, the most depleted construct in the library was *PDCD1*, which encodes the co-inhibitory receptor PD1. Constructs identified as significantly enriched in tumour-infiltrating T cells included MYCN(p. P44L), a fusion of CARD11 and PIK3R3, CCND3(p.P284S), wild-type MYCN, STAT3(p.G618R) and RLTPR(p.Q575E) (Fig. 1f and Extended Data Fig. 3c).

CARD11–PIK3R3 enhances CBM signalling

In vitro, CCND3(p.P284S) and MYCN(p.P44L) showed antigen-dependent downregulation of NFAT, NF-κB and AP-1 signalling despite increased enrichment in vivo (Extended Data Fig. 3d). Previous work in other cell types suggests[14,15] that these constructs may activate proliferative programs without increasing effector functions. By contrast, CARD11–PIK3R3 showed markedly enhanced NF-κB and AP-1 signalling and IL-2 production, without increasing NFAT or PD1 (Extended Data Fig. 3d). Previous work has suggested that increased signalling through NF-κB and AP-1[16,17] but not NFAT[13] could help to counter T cell dysfunction. Additionally, recent studies have demonstrated improved maintenance of memory phenotypes and effector functions in $CD8^+$ T cell subsets that produce high levels of IL-2[18]. These favourable features led us to select CARD11–PIK3R3 for further testing. CARD11–PIK3R3 was initially reported in a single patient with $CD4^+$ cutaneous T cell lymphoma[2]. Notably, this perturbation linking portions of two genes together would not have been identified by previous screening approaches.

In normal T cells, TCR signalling activates PKCθ, which in turn promotes the assembly of the CARD11–BCL10–MALT1 (CBM) signalosome[19] (Fig. 2a); a complex that is essential for normal T cell activation and function in response to antigen[19]. The CBM complex subsequently has three main outputs: NF-κB and AP-1 transcriptional activity and MALT1 proteolytic activity[19]. At rest, an inhibitory domain prevents CARD11 binding to the other members of the CBM complex. Following TCR signalling, this domain is phosphorylated,

enabling oligomerization of CARD11 protein and recruitment of BCL10–MALT1 filaments to form a functional CBM complex[20]. Although T cell-specific functions have not been elucidated for PIK3R3, it contains two SH2 domains that bind to tyrosine-phosphorylated proteins[21]. The product of the translocation between CARD11 and PIK3R3 results in a gene fusion of the amino-terminal CARD11 protein CARD domain, coiled-coil domain and part of the inhibitory domain with an SH2 domain from the carboxy terminus of PIK3R3 (Fig. 2b). Deletion of the PIK3R3 or the CARD11 component of CARD11–PIK3R3 abolished signalling, suggesting that both partners are required for function (Fig. 2c). The coiled-coil domain and CARD domain, but not the truncated portion of the inhibitory region, of CARD11 are necessary to activate NF-κB (Fig. 2c).

Like wild-type CARD11, CARD11–PIK3R3 induces NF-κB and AP-1 signalling (Extended Data Fig. 3d). Thus, we reasoned that it recruits the CBM complex and would subsequently induce MALT1 paracaspase activity. Western blotting of the canonical MALT1 substrates CYLD and HOIL1 (also known as RBCK1)[22] indicated that CARD11–PIK3R3 increased tonic and antigen-dependent cleavage, which was abrogated in the presence of a MALT1 inhibitor (Fig. 2d).

Next we determined whether wild-type CARD11 and BCL10 are required for the function of CARD11–PIK3R3. In unstimulated, CAR-stimulated and pharmacological TCR-stimulated conditions, we observed a reliance of CARD11–PIK3R3 on BCL10 but not wild-type CARD11 (Fig. 2e). Control cells required both CARD11 and BCL10 for TCR-triggered activation of NF-κB but did not depend on CARD11 for CAR-dependent signalling (Fig. 2e). Signalling was reduced when a point mutation in *BCL10* (p.R28A) that abolishes CARD11–BCL10 interaction[23] was introduced, further highlighting the requirement of CARD11–BCL10 binding for NF-κB signalling (Fig. 2f). Similarly, an alteration in the phospho-tyrosine binding pocket of the PIK3R3 SH2 region[24] significantly reduced NF-κB signalling (Fig. 2g). Together, these data indicate that CARD11–PIK3R3 enhances CBM complex signalling in a manner dependent on BCL10 and PIK3R3 SH2-dependent binding of phospho-tyrosine residues.

CARD11–PIK3R3 enhances CAR T cells

Next we carried out RNA sequencing of human $CD4^+$ and $CD8^+$ T cells with and without antigen (Supplementary Table 2). Principal component analysis demonstrated that the greatest transcriptional differences were induced by CAR-dependent stimulation, suggesting that CARD11–PIK3R3 expression is not sufficient to cause a fully activated phenotype (Extended Data Fig. 5a). A total of 43 genes were significantly upregulated in both $CD4^+$ and $CD8^+$ T cells following CAR stimulation (Fig. 3a), including activation markers (*IL2RA*), cytokines (*IFNG*, *TNF*, *IL4*, *IL5* and *IL13*), chemokines (*CCL4*) and co-stimulatory molecules (*ICOS* and *TNFRSF4* (which encodes OX40)). Several of these genes, such as *ICOS*[25] and *TNFRSF4*[26], have previously been suggested to improve anti-tumour responses. CARD11–PIK3R3-expressing $CD4^+$ T cells were enriched for gene signatures related to cell cycle. By contrast, $CD8^+$ T cells were enriched most for RNA metabolism, cytokine signalling and translation signatures (Fig. 3b). Consistent with our

biochemical analyses, pathway analysis identified enrichment of NF-κB, AP-1 and MALT1 paracaspase signatures[27] (Fig. 3b).

Owing to upregulation of proliferation-associated gene pathways in $CD4^+$ T cells, we next assayed cytokine-independent growth in primary CAR T cells. CARD11–PIK3R3 improved the expansion of CAR T cells in the presence of IL-2; however, removal of IL-2 either early or late in the culture led to T cell contraction (Extended Data Fig. 4a–c).

Activation marker expression was consistent with our RNA-sequencing data; CD25 (*IL2RA*) and ICOS were significantly upregulated in both $CD4^+$ and $CD8^+$ CARD11–PIK3R3-expressing CAR T cells (Fig. 3d and Extended Data Fig. 5b). Similarly, expression of ICOS was elevated in CARD11–PIK3R3-expressing CD28z-CAR T cells (Extended Data Fig. 5c). CARD11–PIK3R3 increased basal transcriptional activity of NF-κB in Jurkat cells; however, it did not induce significantly higher expression of activation markers in primary $CD8^+$ T cells compared to that of untransduced controls, although $CD4^+$ T cells transduced with CARD11–PIK3R3 did have increased ICOS expression (Extended Data Fig. 5d). These data, in conjunction with the lack of IL-2-independent growth, suggest that CARD11–PIK3R3 is not sufficient to cause antigen-independent proliferation.

Additionally, CARD11–PIK3R3 induced higher secretion of IL-2, IFNγ, TNF and the T_H2 cytokine IL-5 in $CD8^+$ BBz-CAR T cells (Fig. 3d). Unexpectedly, cytokine secretion was substantially increased in $CD8^+$ CAR T cells more than in $CD4^+$ CAR T cells, despite being originally observed in a $CD4^+$ T cell cancer (Fig. 3d). Similar, although non-significant, trends were observed in $CD8^+$ T cells with a CD28z-CAR (Extended Data Fig. 5e). Notably, cytokine secretion was antigen dependent (Extended Data Fig. 5f).

Next we determined how CARD11–PIK3R3 affects CAR T cell cytotoxicity. Tumour microenvironments often lack pro-survival cytokines required by cytotoxic T cells, such as IL-2[28]. Therefore, we co-cultured transduced $CD8^+$ T cells with CD19-K562 cells for 2 weeks with or without supplementary IL-2. With IL-2, both CARD11–PIK3R3 CD19-BBz CAR T cells and CD19-BBz CAR T cells alone were able to efficiently clear the CD19-K562 targets. However, without supplementary IL-2, only CARD11–PIK3R3-expressing CAR T cells cleared target cells. In one donor, CAR T cells failed to fully eliminate the target cells even with IL-2; however, the addition of CARD11–PIK3R3 enabled tumour cell clearance with or without IL-2 (Fig. 3e). This suggests that CARD11–PIK3R3 may rescue the cytotoxic capacity of potentially clinically relevant poor-quality donor-derived T cells. Less marked differences in cytotoxicity were observed for the CD19-CD28z-CAR T cells, which may be a result of the known propensity for CD28z-CAR T cells to drive more IL-2 production[29] (Extended Data Fig. 5g). However, at every effector-to-target ratio assessed, CARD11–PIK3R3-expressing CAR T cells, regardless of the co-stimulatory domain, exhibited superior control of tumour cell growth (Extended Data Fig. 5h,i). CARD11–PIK3R3 also increased expansion of both BBz and 28z-CAR T cells after multiple stimulations (Extended Data Fig. 5j), suggesting greater antigen-dependent proliferative potential.

We next determined whether CARD11–PIK3R3 promotes the therapeutic efficacy of CD19-BBz-CAR T cells in a $CD19^+$ Nalm6 xenograft leukaemia model. When the TCR was expressed, CARD11–PIK3R3-expressing CAR T cells controlled Nalm6 leukaemia, but mice experienced lethal weight loss consistent with accelerated graft-versus-host disease (Extended Data Fig. 6a–d), which can occur in xenograft experiments with TCR-replete products[30]. When the TCR gene was knocked out, we were able to show that CARD11–PIK3R3 CAR T cells eliminated Nalm6 leukaemia with 100% survival at 33 days. At these doses, control CAR T cells failed to control Nalm6 leukaemic burden (median survival 24 days; Fig. 4a).

Improved efficacy of CD19-BBz-CAR T cells was also observed at higher doses of 7×10^6 CAR^+ T cells, for which four out of seven control CD19-BBz-CAR-treated animals that initially controlled tumour eventually relapsed whereas seven out of seven CARD11–PIK3R3 CD19-BBz-CAR T cell-treated animals did not relapse (Fig. 4b and Extended Data Fig. 7a). Notably, CARD11–PIK3R3 T cells without the CD19-CAR had no anti-tumour effect, demonstrating that antigen is required for tumour clearance (Fig. 4b). Nalm6-bearing animals that controlled tumours with CAR or CARD11–PIK3R3 CAR T cell treatment gained weight over the course of 100 days, losing weight only when Nalm6 relapse occurred, suggesting that high doses of CARD11–PIK3R3 CAR T cells are well tolerated (Fig. 4b and Extended Data Fig. 7b). Similarly, non-tumour-bearing mice tolerated high doses of control T cells, CARD11–PIK3R3 T cells, CAR T cells and CARD11–PIK3R3 CAR T cells (Extended Data Fig. 7c). Finally, following Nalm6 tumour rechallenge of CARD11–PIK3R3 CAR T cell-treated animals (excluding two animals with symptoms of graft-versus-host disease and one animal that died tumour negative), we found that CAR T cell-treated animals succumbed to Nalm6 disease at a rate similar to that of naive age-matched controls, whereas CARD11–PIK3R3 CAR T cells prevented Nalm6 growth (Extended Data Fig. 7d). These data indicate that CARD11–PIK3R3 enhances therapeutic efficacy while maintaining safety, even at high T cell doses.

We next dosed Nalm6-bearing mice with 4×10^5 CD19-CD28z-CAR T cells or CARD11–PIK3R3 CD19-CD28z-CAR T cells (Extended Data Fig. 8a). Control CAR T cell-treated animals succumbed to disease, whereas CARD11–PIK3R3 CAR T cells cleared an initial Nalm6 tumour challenge, and a rechallenge (injected on day 77 post initial tumour implantation; Fig. 4c,d and Extended Data Fig. 8b). Therefore, the anti-tumour efficacy of CARD11–PIK3R3 expression improves in vivo functions of both 28z and BBz CARs.

We then evaluated CARD11–PIK3R3 in a subcutaneous model of mesothelioma (M28), targeting the tumour-associated antigen MCAM[31]. CARD11–PIK3R3 MCAM-CD28z-CAR T cell-treated animals exhibited enhanced M28 tumour control over the course of approximately 70 days, without exhibiting signs of toxicity or weight loss (Fig. 4e and Extended Data Fig. 8c,d). Therefore, CARD11–PIK3R3 also safely improves the long-term therapeutic efficacy of human CAR T cells in vivo in solid tumour settings.

We next sought to determine whether CARD11–PIK3R3 improves CAR T cell efficacy in an immunotherapy-refractory, fully immuno-competent in vivo setting with an intact immunosuppressive tumour microenvironment[32]. To accomplish this, we expressed human

CD19 on B16-F10 melanoma (B16-hCD19$^+$) and transduced CD45.2$^+$ OT-I CD8$^+$ T cells with the human CD19-targeted mouse BBz CAR with or without human CARD11–PIK3R3 (Extended Data Fig. 8e). Animal weight was maintained throughout the study (Extended Data Fig. 8f). At 5 days post adoptive transfer, we observed a significantly higher number of CARD11–PIK3R3-expressing CAR T cells in the tumour and spleen, suggesting greater in vivo expansion and/or persistence of CARD11–PIK3R3 CD19-BBz-CAR T cells (Fig. 4f and Extended Data Fig. 8g). Furthermore, CARD11–PIK3R3 CAR T cells exhibited improved tumour control compared to untransduced or CD19-BBz CAR T cells (Fig. 4g). Tumours eventually relapsed in the CARD11–PIK3R3-treated mice after initial regression. In a repeated study, CD19-BBz-CAR-treated tumours maintained CD19 expression, whereas CARD11–PIK3R3 CD19-BBz-CAR T cell-treated tumours were uniformly CD19 negative, suggesting antigen loss as the mechanism of relapse (Extended Data Fig. 8h). Overall, CARD11–PIK3R3 CD19-BBz CAR T cell therapy resulted in significantly improved survival compared to CD19-BBz-CAR T cell therapy (Fig. 4g). Notably, this anti-tumour activity was achieved without lymphodepletion. Lymphodepletion regimens increase the availability of homoeostatic cytokines that signal through the common gamma chain and thus have been shown to significantly improve CAR T cell engraftment and efficacy[33].

CARD11–PIK3R3 enhances TCR T cells

We next assessed the efficacy of the CARD11–PIK3R3 T cells in a TCR-transgenic tumour model. We used the B16-F10 melanoma model wherein the melanoma cells express chicken ovalbumin[34] (OVA; Fig. 5a). CD45.1$^+$ OT-I CD8$^+$ T cells were transduced with either control (GFP) or CARD11–PIK3R3 (mCherry) retroviruses, enabling tracking of adoptively transferred cells in CD45.2$^+$ C57BL/6J hosts bearing B16-OVA melanoma tumours.

First we used a dual-transfer system to determine the relative fitness of cells expressing control vector or the CARD11–PIK3R3[35]. We used CD45.1$^+$ OT-I T cells in which approximately 10% of the cells were mCherry$^+$ (corresponding to CARD11–PIK3R3-expressing cells), which were mixed with control cells expressing GFP. Notably, we observed a 145-fold increase in cell number (normalized to input) of CARD11–PIK3R3-expressing cells compared to control cells among the tumour-infiltrating lymphocytes (TILs) 7 days following transfer (Fig. 5b). This corresponded to a significantly increased fraction of transferred cells among total CD8$^+$ T cells, even without normalization to input numbers (Extended Data Fig. 9a). Therefore, within the same tumour microenvironment, CARD11–PIK3R3 markedly improves intra-tumoural accumulation. Unexpectedly 4 out of 5 tumours cleared by day 21 when treated with a mixed population graft (containing 10% CARD11–PIK3R3-expressing cells), preventing characterization of TILs at a later time point (Extended Data Fig. 9b). Enhanced competitive accumulation of CARD11–PIK3R3 was confirmed in a second TCR-transgenic mouse model, using pmel-1 T cells (which recognize gp100, an endogenous melanoma antigen) against B16-F10 tumours (Extended Data Fig. 9c–e). Using the BCL10-binding-deficient mutant in this model, we further demonstrated a requirement of BCL10 binding by CARD11–PIK3R3 for the in vivo phenotype (Extended Data Fig. 9c–e).

We next characterized the phenotype of cells following adoptive transfer of either CARD11–PIK3R3- or vector control-transduced OT-I cells. At 7 days post transfer of 1×10^6 CARD11–PIK3R3 OT-I cells, CARD11–PIK3R3 OT-1 were significantly enriched in the tumour, spleen and tumour-draining lymph node (Fig. 5c and Extended Data Fig. 9f). To assess mechanisms, we carried out functional analysis of CARD11–PIK3R3 OT-I TILs. CARD11–PIK3R3 increased the expression of the stemness-associated transcription factor TCF1 in TILs (Fig. 5c). However, TCF1 was not elevated in spleen or tumour-draining lymph node, suggesting tumour-specific remodelling of T cell phenotype (Extended Data Fig. 9g). Moreover, CARD11–PIK3R3 TILs showed increased poly-functionality. CARD11–PIK3R3 increased the production of TNF, IFNγ and IL-2 individually and collectively (Fig. 5d and Extended Data Fig. 9h). Together, these results indicate that CARD11–PIK3R3 expression promotes the intra-tumoural accumulation of highly functional, stem-like T cells.

Finally, we assessed therapeutic efficacy. At 12 days post tumour injection, mice were treated with PBS control or 2×10^6 OT-I cells with or without CARD11–PIK3R3, without preconditioning or lymphodepletion. CARD11–PIK3R3 OT-I T cells mediated significantly enhanced control of tumour growth (Extended Data Fig. 9i). Additionally, CARD11–PIK3R3 OT-I cells promoted prolonged overall survival. Strikingly, 60% of mice (3/5) receiving CARD11–PIK3R3 achieved complete clearance of tumours at more than three months following tumour challenge, at which point no PBS-treated or control OT-I T cell-treated mice survived (Extended Data Fig. 9i). One of the CARD11–PIK3R3-treated mice died with a skin ulceration but without tumours. We did not observe weight loss, ataxia or other systemic symptoms in the CARD11–PIK3R3-treated mice compared to controls (Extended Data Fig. 9j).

As the competition experiment suggested potency at low doses of transferred T cells, we carried out a cell dose–response experiment. We compared the therapeutic efficacy of 20,000 and 100,000 CARD11–PIK3R3-positive OT-I cells against 2×10^6 control OT-I cells in B16-OVA tumour-bearing mice, again without lymphodepletion. Strikingly, CARD11–PIK3R3 enabled superior tumour control with both a 20-fold (4/4 cleared) and 100-fold (5/5 cleared) lower dose than control cells (Fig. 5e). These animals treated with low cell doses or naive controls were rechallenged with B16-OVA tumour cells in the contralateral flank. Low doses of CARD11–PIK3R3 OT-I T cells were sufficient to confer significantly better protection against tumour development compared to naive, untreated mice (Fig. 5e).

We next sought to assess CARD11–PIK3R3 efficacy in a human TCR model. Using HLA-C*08:02-over-expressing SNU-1 gastric carcinoma cells that harbour a *KRAS* (p.G12D)[36] mutation and a clinically validated TCR against HLA-C*08:02-presented KRAS(p.G12D), we observed significantly enhanced tumour clearance with CARD11–PIK3R3 expression (Fig. 5f). Therefore, CARD11–PIK3R3 expression enhances the function of both human and mouse therapeutic TCR cells. Together, these data indicate that CARD1–PIK3R3-expressing T cells have superior therapeutic function in vivo in several immunotherapy-refractory tumour models, including CAR- and TCR-transgenic-based models.

To address concerns of toxicity or transformation, we monitored mice from Fig. 5e and Extended Data Fig. 9i for up to 418 days after T cell transfer (Extended Data Fig. 10a). CARD11–PIK3R3 OT-I T cell-treated animals gained weight similarly to published controls (Extended Data Fig. 10b). Necropsy carried out on three mice on day 240 after T cell transfer revealed spleens of normal weight and gross appearance (Extended Data Fig. 10c,d). Additionally, CARD11–PIK3R3 OT-I T cells made up less than 1% of total $CD8^+$ T cells in the spleen and blood (Extended Data Fig. 10e). We carried out haematoxylin and eosin staining of spleen, lymph nodes and common extra-nodal sites of lymphoma. Pathology review failed to identify any evidence of nuclear atypia, destruction of normal cellular architecture or neoplastic disease (Extended Data Fig. 10f). Tail bleeds of the remaining CARD11–PIK3R3 OT-I-treated animals 330–418 days after adoptive transfer revealed that CARD11–PIK3R3 OT-I T cells were present at less than 1% of the overall $CD8^+$ population (Extended Data Fig. 10g–j). These data suggest contraction of CARD11–PIK3R3 OT-I T cells after initial inoculation or tumour rechallenge without evidence of malignant transformation in vivo over long time periods.

Discussion

By screening T cell neoplasm mutations through both in vitro and in vivo arrayed assays, we identified how individual mutations can tune T cell signalling, improve cytotoxic T cell functions and promote in vivo accumulation. This approach identified a new gene fusion, *CARD11–PIK3R3*, which markedly enhances therapeutic T cell function and efficacy. CARD11–PIK3R3, although discovered in a $CD4^+$ T cell lymphoma, had outsized effects in $CD8^+$ T cells, increasing function in vitro and tumour control in vivo in xenograft and syngeneic models. Future work is required to better understand the mechanistic differences of CARD11–PIK3R3 signalling in $CD4^+$ and $CD8^+$ T cells, as well as PIK3R3 targets in CARD11–PIK3R3-expressing cells.

Moreover, our results implicate the CBM signalosome as a key regulator of therapeutic T cell function. Several individual outputs of CBM signalling such as inducing AP-1 and NF-κB transcriptional activity[16,17], and downregulation of the MALT1 cleavage substrates Regnase 1 (also known as ZC3H12A) and roquin (also known as RC3H1)[35,37], have each been implicated independently as putative potency enhancements. This raises the possibility that each approach addresses a relative deficiency of CBM signalling in TILs. CARD11–PIK3R3 expression represents a powerful solution to enhance each of these separate CBM outputs simultaneously. Further investigation of T cell mutations in the context of adoptively transferred T cells has the promise to both improve cellular therapies and elucidate new T cell biology.

It is important to consider how to optimally ensure the safety of T cell therapeutics combined with CARD11–PIK3R3 or other T cell lymphoma mutations. Individual T cell lymphoma mutations generally do not cause lymphomagenesis. They are often found in rogue cells that contribute to autoinflammatory or autoimmune disease[5]. Moreover, numerous studies have used knockout of genes encoding T cell lymphoma tumour suppressors to enhance T cell therapy without evidence of malignant transformation, including knockout of *PDCD1* in a phase I trial[10].

Nonetheless, while the manuscript was in press, the US Food and Drug Administration (FDA) announced an investigation[38] following reports “of T-cell malignancies, including chimeric antigen receptor CAR-positive lymphoma, in patients who received treatment with BCMA- or CD19-directed autologous CAR T cell immunotherapies”. The FDA report includes 12 observed cases in the FDA databases among >30,000 patients treated worldwide, suggesting an incidence of <0.1%, which is significantly lower than the risk (4–16%)[39] of other non T cell malignancies that are likely to be unrelated to the CAR T product, including solid tumours and myeloid malignancies.

Details about the T cell lymphoma diagnosis have not yet been revealed. Some of the cases are CAR^-, suggesting that they do not arise from the CAR T product itself. These cases are probably due to the high pre-existing risk of sporadic second primary malignancies found in patients with B cell malignancies (even those who do not receive CAR T)[40]. In particular, these patients with B cell malignancies (even without CAR T treatment) have a higher risk specifically of T cell lymphomas[41]. A single case of a patient developing CAR^+ T cell lymphoma after receiving a BCMA-targeted CAR therapy has been reported, which suggested a role for pre-existing mutations before CAR manufacture, including *JAK3* and *TET2* mutations[42].

Although the source of this particular potency enhancement may suggest risk, CARD11–PIK3R3 has potential safety advantages over other approaches. Unlike the effects of CRISPR knockout of genes encoding putative tumour suppressors or constitutive *IL7R* (NCT04099797), the phenotypic effects of CARD11–PIK3R3 are antigen dependent, minimizing the risk of autonomous proliferation. In addition, this potency enhancement seems to obviate the need for lymphodepleting chemotherapy, which has been shown to be mutagenic and increase risk of secondary malignancies[43]. Our long-term in vivo xenograft and syngeneic studies, carried out in multiple models and at high T cell doses, showed no signs of lymphomagenesis, even at 418 days after adoptive T cell transfer. These data suggest that the risk of malignant transformation could be measured and managed.

Last, we have developed engineering strategies to further mitigate the potential risk of lymphomagenesis and/or autoimmunity or graft-versus-host disease. First, the risk for pathological signalling from the endogenous TCR can be mitigated by strategies to knockout the gene expressing it. Second, to ensure safety, *CARD11–PIK3R3* or other mutations may be candidates for controlled expression (for example, with synNotch or synthetic intramembrane proteolysis receptor circuits), which we have previously used for antigen-specific transcriptional regulation of payloads[44–46]. Third, gene-editing enzymes can enable precise insertion of the *CARD11–PIK3R3* into the genome and thus prevent random integration into putative tumour suppressors. Fourth, cells can be engineered with additional safety measures such as suicide switches to enable CAR T depletion if medically necessary.

Methods

Vector construction

Receptors were built by fusing the CD19 single-chain variable fragment[47] to the corresponding receptor scaffold and intracellular tail. All receptors contain an N-terminal

CD8α signal peptide (MAL-PVTALLLPLALLLHAARP) for membrane targeting and a Flag tag (DYK-DDDDK) for easy determination of surface expression with anti-Flag PE (Biolegend 637310). In some cases, the receptors additionally contained a T2A self-cleaving sequence followed by a tNGFR sequence, used in downstream applications for T cell isolations. The receptors were cloned into a modified pHR'SIN:CSW vector containing a PGK promoter for all primary T cell experiments. Wild-type genes of the mutation library were ordered as plasmids through DNASU, and point mutations were introduced through PCR. Some mutated genes were synthesized by Twist. Wild-type or mutated gene fragments were cloned into a modified pHR'SIN:CSW vector containing a PGK promoter followed by a T2A self-cleaving sequence, a unique bar-code and the fluorescent tag mCherry used to identify transduced cells. Wild-type or mutant gene fragments were cloned through an *Sbf1* site in the multiple cloning site 3′ to the PGK promoter sequence. All constructs were cloned through Infusion cloning (Clontech No. ST0345) or Gibson assembly.

Primary human T cell isolation and culture

Primary $CD3^+$, $CD4^+$ and $CD8^+$ T cells were isolated from anonymous donor blood after apheresis by negative selection (Biolegend Nos. 480131, 480130 and 480129). Blood was obtained from Blood Centers of the Pacific (San Francisco, CA) as approved by the University Institutional Review Board. T cells were cryopreserved in RPMI-1640 (University of California, San Francisco cell culture core) with 20% human AB serum (Valley Biomedical, No. HP1022) and 10% dimethylsulfoxide. After thawing, T cells were cultured in human T cell medium consisting of X-VIVO 15 (Lonza No. 04-418Q), 5% human AB serum and 10 mM neutralized *N*-acetyl l-cysteine (Sigma-Aldrich No. A9165); for in vitro assays, medium was supplemented with 30 units per millilitre of IL-2 (NCI BRB Preclinical Repository), and for experiments involving TCR gene knockout, human T cell medium was supplemented with 100 units per millilitre of IL-7 (Miltenyi No. 130-095-362) and 100 units per millilitre of IL-15 (Miltenyi No. 130-095-765).

Lentivirus production and human T cell transduction

Pantropic VSV-G-pseudotyped lentivirus was produced through transfection of Lenti-X 293T cells (Clontech No. 11131D) with a pHR'SIN:CSW transgene expression vector and the viral packaging plasmids pCM-VdR8.91 and pMD2.G using Mirus TransIT-Lenti (Mirus No. MIR 6606). Primary T cells were thawed and stimulated with Human T-Activator CD3/CD28 Dynabeads (Life Technologies No. 11131D) at a 1:3 cell/bead ratio. At 48 h, viral supernatant was collected and the primary T cells were exposed to the virus for 24 h. In some cases, previously prepared and frozen concentrated virus was used in place of fresh. At day 5 post T cell stimulation, the Dynabeads were removed, T cells were sorted, and the T cells were expanded until day 10–14 when they were rested and could be used in in vitro or in vivo assays. T cells were sorted for assays with a Beckton Dickinson FACS ARIA II.

TCR gene knockout of lentivirally transduced human T cells

For TCR gene knockout experiments, primary T cells were activated and transduced as indicated above. At 24 h post transduction, virus and Dynabeads were removed, and cells were rested for 24 h, and then resuspended at 1×10^6 cells per millilitre in P3 electroporation buffer (Lonza No. V4SP-3960) with sgRNA

(CAGGGUUCUGGAUAUCUGU) targeting the human *TRAC* locus and Cas9. A 23 μl volume of this mixture was aliquoted to each well of a 96-well nucleofection plate (Lonza No. V4SP-3960) and immediately electroporated using a 4D Lonza Nucleofector with program EH115. Cells were resuspended in pre-warmed human T cell medium and recovered for 30 min in the incubator before being transferred to culture. Electroporated cells were assessed for TCR gene knockout and lentiviral transduction through flow before injection into mice.

Cell lines

The cancer cell lines used were K562 myelogenous leukaemia cells (ATCC No. CCL-243), Jurkat cells (clone E6-1, ATCC No. TIB-152), B16-F10 melanoma cells (ATCC No. CRL-6475), M28 epithelioid cells (originally obtained from Dr. Brenda Gerwin's laboratory at the National Cancer Institute), A549 lung epithelial carcinoma cells (ATCC No. CCL-18) and SNU-1 (ATCC No. CRL-5971). K562 and A549 cells were lentivirally transduced to stably express human CD19. CD19 levels were determined by flow cytometry (Biolegend, clone HIB19). A549 cells were additionally transduced to express the nuclear stain mKate2. SNU-1 cells were transduced with HLA-C*08:02. Jurkat cells were transduced with retroviruses encoding fluorescent reporter constructs[48] (Addgene 118095, 118094 and 118031) and stimulated with phorbol myristate acetate and ionomycin to sort a line with high induction of each reporter. To enable screening with our mCherry-expressing lentiviral constructs, an iRFP fluorescent reporter was subcloned to replace mCherry in the previously described AP-1–mCherry construct. Triple-reporter cells were then transduced with a CD19-28z-CAR or CD19-BBz-CAR. Jurkat, SNU-1 and K562 cells were cultured in RPMI + 10% FBS with penicillin/streptomycin and sodium pyruvate. B16-OVA, B16-F10 and A549 cells were cultured in DMEM + 10% FBS with penicillin and streptomycin. All cell lines were routinely tested for mycoplasma contamination (Southern Biotech).

In vitro primary T cell assays

For in vitro co-culture assays, transduced primary T cells were co-cultured with target cells at the indicated effector-to-target ratios and co-culture time courses. For Luminex assays, cells were co-cultured in medium lacking exogenous IL-2, and supernatants were collected 48 h after start, frozen at −80 °C and sent for analysis to Eve Technologies. For repeat stimulation assay, transduced T cells were co-cultured on the adherent CD19-expressing A549 cell line, and after 1 week T cells were removed from co-culture without disturbing adherent cells, counted and replated on CD19-expressing A549 cells seeded 24 h before. For co-culture assays carried out over a period of days to weeks, medium was supplemented regularly. All primary T cell in vitro assays were carried out with three donors, unless otherwise noted in the figure legend.

Flow cytometry

For all in vitro primary T cell assays, cells were washed with PBS 2% FBS twice, stained with surface staining markers (diluted 1:200) at room temperature for 20 min, washed twice and resuspended in PBS 2% FBS with DRAQ7 (diluted 1:1,000) before analysis on a Beckton Dickinson FACSymphony X-50 flow cytometer.

Jurkat reporter screening and analysis

CAR triple-reporter Jurkat cells were transduced in 96-well plate format with individual T cell mutation lentiviruses. At 48 h post transduction, cells were plated at approximately a 1:1 ratio with K562 or CD19-K562 cells. Plates were spun at 300*g* for 2 min to promote interaction of CAR cells and target cells. Following 24 h of co-culture, supernatants were removed for IL-2 ELISA (ELISA MAX Deluxe Set Human IL-2, Biolegend), and cells were washed in FACS buffer (PBS + 2% FBS) and analysed by FACS. For the BBz-CAR screen, cells were stained with anti-PD1 (Biolegend, clone EH12.2H7) before FACS analysis. Each screen was carried out in biological replicate with separate lentiviral transductions. For analysis, the percentage positive for each reporter in each condition (that is, each CAR and co-culture cell type) was compared to the mCherry-only controls and the corresponding wild-type gene control when available by *t*-test followed by Bonferroni correction. *z* scores were calculated for each condition as $(x - \mu)/\sigma$ (in which x is the observed value, μ is the mean, and σ is the standard deviation). Constructs were excluded if insufficient mCherry$^+$ cells were obtained for FACS analysis or if they failed sequencing verification.

In vivo screening and analysis

Human CD3$^+$ T cells were lentivirally co-transduced with a CD19-BBz CAR with tNGFR and the mutant construct library in an arrayed fashion. CD3$^+$ T cells were assessed through flow for CD19-BBz CAR (Flag) and mutant construct (mCherry) expression. T cells were pooled on the basis of mCherry expression and sorted for a purified dual-positive population. A total of 6×10^6 library T cells were injected to 15 CD19-K562 tumour-bearing animals. T cells were isolated from the tumour by positive selection using the tNGFR (CELLection Biotin Binder Kit) at 7, 14 and 21 days post injection. gDNA was isolated from these T cells (NucleoSpin Tissue, Machery-Nagel), and PCR amplification was carried out to amplify the bar-code region, followed by a subsequent PCR step to add Illumina bar-codes and adapters to the products. These products were then pooled at 1:1 molar ratio, and run on a MiniSeq 75 cycle cartridge using the standard manufacturer protocols. MAGeCK software (https://sourceforge.net/projects/mageck/) was utilized to identify significantly enriched or depleted bar-codes. Constructs with fewer than 10^2 reads in the pre-injection sample were excluded from analysis.

Bulk RNA-sequencing and analysis

For bulk RNA-sequencing, CD4$^+$ or CD8$^+$ T cells from three independent healthy donors transduced with the indicated constructs were either unstimulated or stimulated through co-culture with CD19-expressing A549 cells for 8 h. RNA was then isolated (Nucleospin RNA XS, Machery-Nagel) and cDNA libraries were constructed using the SMART-Seqv4 Ultra Low Input RNA Kit (Takara Bio) and Nextera XT (Illumina). Sequencing reads were aligned using STAR, transcripts were quantified using HT-Seq, and differentially expressed genes were identified using DESeq2 as previously described[8].

Immunoblot analysis

Jurkat cells ($1–5 \times 10^6$) were pre-treated for 30 min with the MALT1 inhibitor Z-VRPR-FMK (75 μM) or vehicle control. Cells were then treated with phorbol myristate acetate

and ionomycin as indicated for 2 h. Whole-cell lysates were generated and analysed by immunoblotting with the following antibodies: anti-HOIL1 (Millipore Sigma, MABC576), anti-CYLD (Santa Cruz, sc-74435) and anti-β-actin (Cell Signaling Technologies, 4967).

CARD11 and *BCL10* CRISPR knockout

CRISPR knockout was carried out in triple-reporter Jurkat cells using the SE Cell Line 4D-Nucleofector Kit (Lonza). A total of 1×10^6 cells were nucleofected with Cas9 alone or ribonuclear protein complexes of Cas9 with *CARD11* gRNA (CAATGACCTTACACTGACGC) or *BCL10* gRNA (TCGCCGAATAGATTCAACAA).

Mouse T cell purification and retroviral transduction

$CD8^+$ T cells were isolated from the spleens of $CD45.1^+$ or $CD45.2^+$ OT-I mice using a mouse $CD8^+$ T cell isolation kit (Stemcell Technologies, No. 19853) or mouse pan $CD3^+$ T cell isolation kit (Biolegend, No. 480031). T cells were then cultured with 100 U ml^{-1} recombinant human IL-2 (Peprotech), anti-CD3e (1 μg ml^{-1}) and anti-CD28 (0.5 μg ml^{-1}) overnight. For CAR experiments, T cells were stimulated overnight with anti-CD3 and anti-CD28 beads (ThermoFisher). Retroviral supernatants were added to T cells in plates coated with RetroNectin (Takara), and spinduction was carried out for 1 h at 2,000 r.p.m. at 30 °C. Following transduction, T cells were resuspended and cultured in fresh medium containing 100 U ml^{-1} IL-2 until adoptive transfer. Transduction efficiency was determined by flow cytometry before adoptive transfer.

In vivo xenograft assays

NOD.Cg-Prkdc^{scid} Il2rg^{tm1Wjl}/SzJ (NSG) mice were dosed with tumour cells through subcutaneous injection (solid tumour) or tail vein injection (Nalm6). Mice with a similar-sized tumour burden were randomized to receive treatments of CAR T cells. Engineered or control T cells were dosed through retro-orbital injection. Control T cells were dosed equivalent to the highest total T cell dose in other treatment groups. Subcutaneous tumours were measured with digital callipers twice weekly, and tumour volume was calculated using the following formulae: $(\text{length} \times \text{width}^2)/2$ (CD19-K562 and M28) or $\text{length} \times \text{width} \times [(\text{length} \times \text{width})^{0.5}] \times \pi/6$ as previously described[35] (SNU-1). For subcutaneous tumours, death was defined as a progressively growing tumour that reaches 15 mm (SNU-1) or 20 mm (CD19-K562 and M28) in its longest axis, a tumour volume that reaches 2,000 mm^3 or a tumour that develops ulceration or necrosis. For the Nalm6 leukaemic model, death was defined as hind limb paralysis, poor body score or loss of 15% or more of body weight, whichever occurred first. Animal drinking water was supplemented with Clavomox to prevent bacterial infections. Experiments were carried out in accordance with the protocols approved by the University of California, San Francisco Institutional Animal Care and Use Committee.

B16 melanoma tumour model

For TCR experiments, female C57BL/6 mice aged 6–8 weeks were injected subcutaneously with 5×10^5 B16-OVA or B16-F10 melanoma cells. Mice with similar-sized tumours were randomized to receive treatments of OT-I or pmel-1 T cells. A 100 μl volume of T

cells (or PBS control) was retro-orbitally injected on day 8–12 post tumour inoculation. For dual-transfer competitive assay and TIL analysis experiments, 1×10^6 T cells were transferred. For anti-tumour efficacy, 2×10^6 T cells were transferred. For dose–response experiments, the indicated numbers of cells were transferred. For rechallenge experiments, B16-OVA cells were injected subcutaneously on the opposite flank. Tumour lengths and widths were determined every 2–3 days by digital calliper measurement and tumour volume was calculated as length × width × $[(\text{length} \times \text{width})^{0.5}] \times \pi/6$ as previously described[35]. Death was defined as a progressively growing tumour that reaches 15 mm in its longest axis or that develops ulceration or necrosis. For anti-tumour efficacy experiments, measurement of tumours and determination of survival endpoint was blinded to experimental condition.

For CAR experiments, male B6.SJL-Ptprca Pepcb/BoyJ mice aged 6–12 weeks were injected subcutaneously with 1×10^5 CD19-B16 melanoma cells. Mice with similar-sized tumours were randomized to receive treatments of CAR T cells. A 100 µl volume of T cells (or PBS control) was retro-orbitally injected on day 12 post tumour inoculation. Control T cells were dosed equivalent to the highest total T cell dose in other treatment groups. Tumour lengths and widths were determined 2–3x per week by digital calliper measurement and tumour volume was calculated using the following formula: $(\text{length} \times \text{width}^2)/2$. Death was defined as a progressively growing tumour that reaches 2,000 mm^3 or 20 mm in its longest axis, whichever comes first.

Experiments were carried out in accordance with protocols approved by the Institutional Animal Care and Use Committee of the University of California, San Francisco and that of Northwestern University.

B16 TIL isolation and analysis

To isolate TILs, B16-F10-OVA tumours were excised, minced and digested using collagenase IV (1 mg ml^{-1}) and DNAseI (50 µg ml^{-1}) for 30 min at 37 °C in a shaking incubator at 200 r.p.m. TILs were filtered through a 70-µM cell strainer; in some cases lymphocytes were isolated over Percoll density centrifugation. For dual-transfer experiments, the isolated TILs were subjected to Fc receptor blocking, live/dead staining (Live/Dead Violet) and surface marker staining for flow cytometric analysis. For intracellular cytokine staining, cells were restimulated ex vivo in medium containing brefeldin and monensin (Invitrogen), phorbol myristate acetate and ionomycin for 4 h. Following Fc blocking, live/dead staining and cell surface marker staining, cells were fixed (Beckton Dickinson CytoFix), permeabilized (Invitrogen 10× Perm) and stained for intracellular proteins.

Mouse necropsy

Necropsy was carried out using protocols outlined by the Northwestern University Center for Comparative Medicine. Three mice were euthanized. Mice and spleens were weighed at the time of necropsy. Half the spleen and blood samples were taken for FACS analysis of transferred cells. After removal of the spleen, the mice were perfused with 10% neutral-buffered formalin. Mouse blood, skin, heart, lung, brain, liver, stomach, kidney, intestine, colon, pancreas, lymph nodes, bone, spleen and bladder were removed and fixed at room

temperature for 48 h in 10% neutral-buffered formalin, followed by 24 h in 70% ethanol. After 24 h in 70% ethanol, all tissues were embedded by the Mouse Histology and Phenotyping Laboratory at Northwestern University. Slides were evaluated by Dr Jared T. Ahrendsen, Director of the Mouse Histology and Phenotyping Laboratory at Northwestern University and Assistant Professor of Pathology at Northwestern University for signs of nuclear atypia, cellular architecture and presence of neoplastic disease.

Extended Data

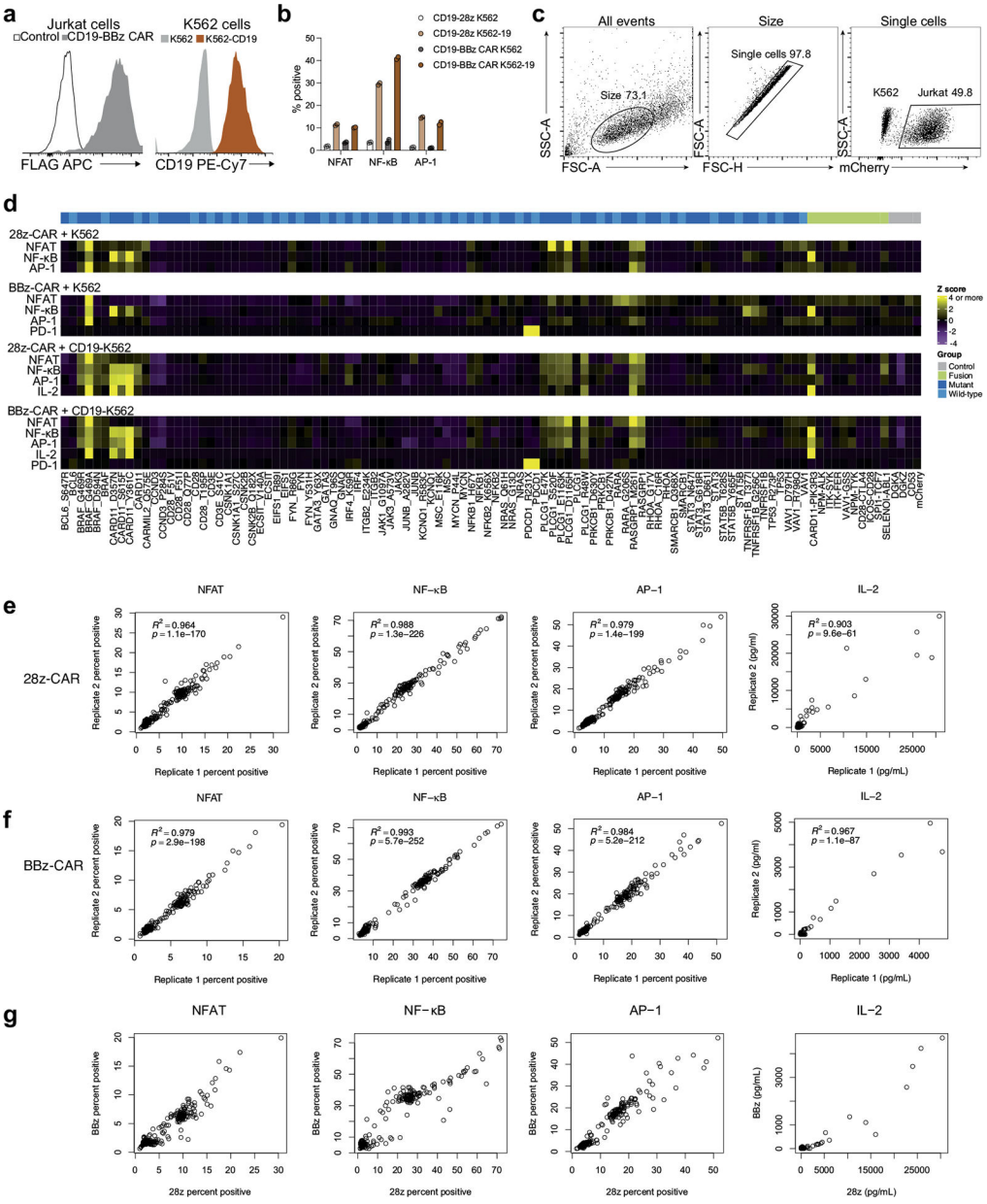

Extended Data Fig. 1 |. In vitro screening of 28z-CAR and BBz-CAR triple reporter Jurkat cells. (**a**) CAR and CD19 expression in cell lines utilized for screening. (**b**) Percent positive for the indicated reporter construct in 28z-CAR or BBZ-CAR transduced Jurkat cells

co-cultured with the indicated cell line (n = 2). (**c**) Gating strategy to identify library construct transduced Jurkat cells in co-culture. (**d**) Heatmaps depicting Z scores in vitro screens. Z scores represent mean of two experimental replicates. Z scores are calculated on a row-by-row basis and thus represent different percentage positive values across different experimental conditions, such as with or without CD19 antigen. (**e-f**) Reproducibility of screening in 28z-CAR Jurkat cells (**e**) or BBz-CAR Jurkat cells (**f**). Each replicate indicates an independent lentiviral transduction of Jurkat cells with T cell mutation screening constructs, statistics determined by simple linear regression. (**g**) Scatterplot indicating CD19–28z CAR (x-axis) and CD19-BBz CAR (y-axis) percent positive for reporter constructs and IL-2 production.

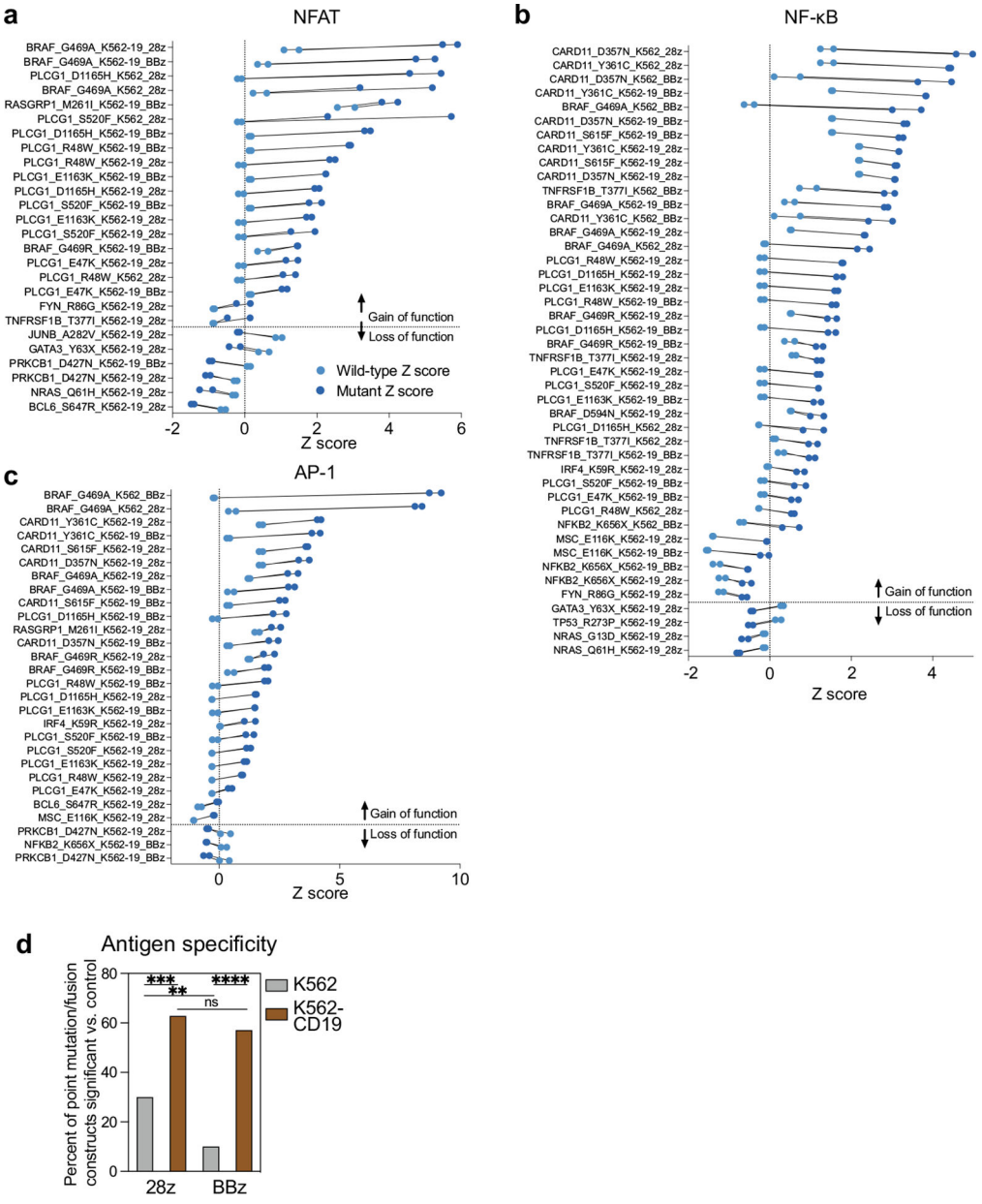

Extended Data Fig. 2 |. Point mutations with statistically significant differences compared to wild-type constructs and antigen specificity of mutations.

(a-c) NFAT, NF-κB, and AP-1 reporter activity. Mutations with a statistically significant difference from the wild-type construct are shown. Each row indicates the mutation construct, co-culture condition and CAR construct. Gain of function indicates mutations which increased reporter activity relative to wild-type, while loss of function refers to mutations with lower reporter activity than the wild-type counterpart. Each dot indicates one biological replicate. (**d**) Percent of constructs with significant effects in the indicated CAR and co-culture condition. ** indicates P value < 0.01, *** indicates P < 0.001, **** indicates P < 0.0001, Chi-squared test.

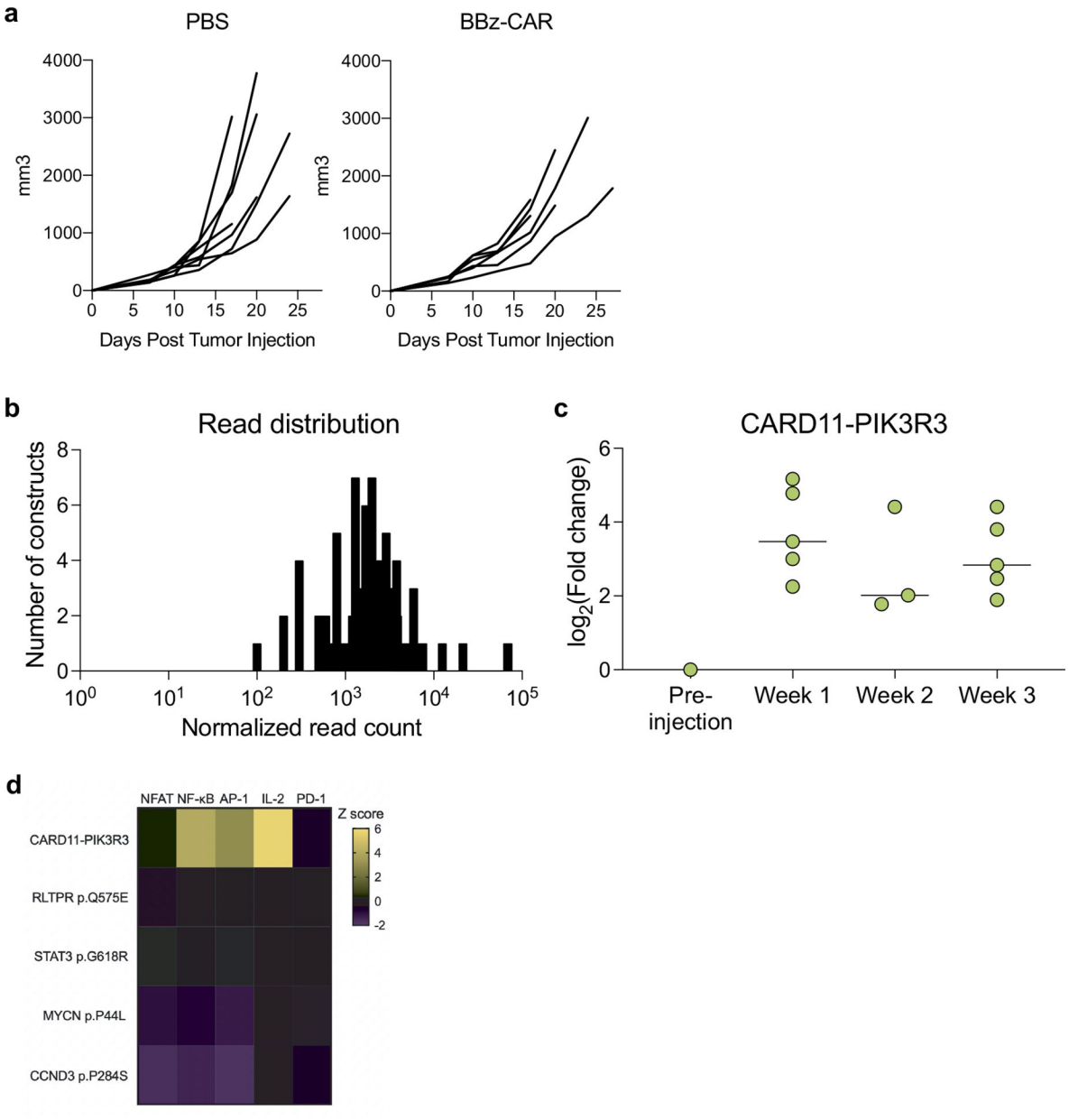

Extended Data Fig. 3 |. Pooled human CAR T cell in vivo persistence screening of T cell mutation library.

(a) Tumor growth curve for mice bearing CD19-K562 subcutaneous tumors treated with vehicle (PBS, control) or 1 × 106 CAR + T cells. **(b)** Histogram of normalized read count distribution of pre-injection constructs. Constructs with a pre-injection normalized read count of $<10^2$ were excluded from analysis. **(c)** Log_2 fold change of CARD11-PIK3R3 normalized reads at each indicated time point in the pooled in vivo experiment (week 1 n = 5, week 2 n = 3, week 3 n = 5). **(d)** In vitro screen Z scores of mutation constructs identified as positive hits from in vivo screening. Z score represents the mean Z score of two experimental replicates.

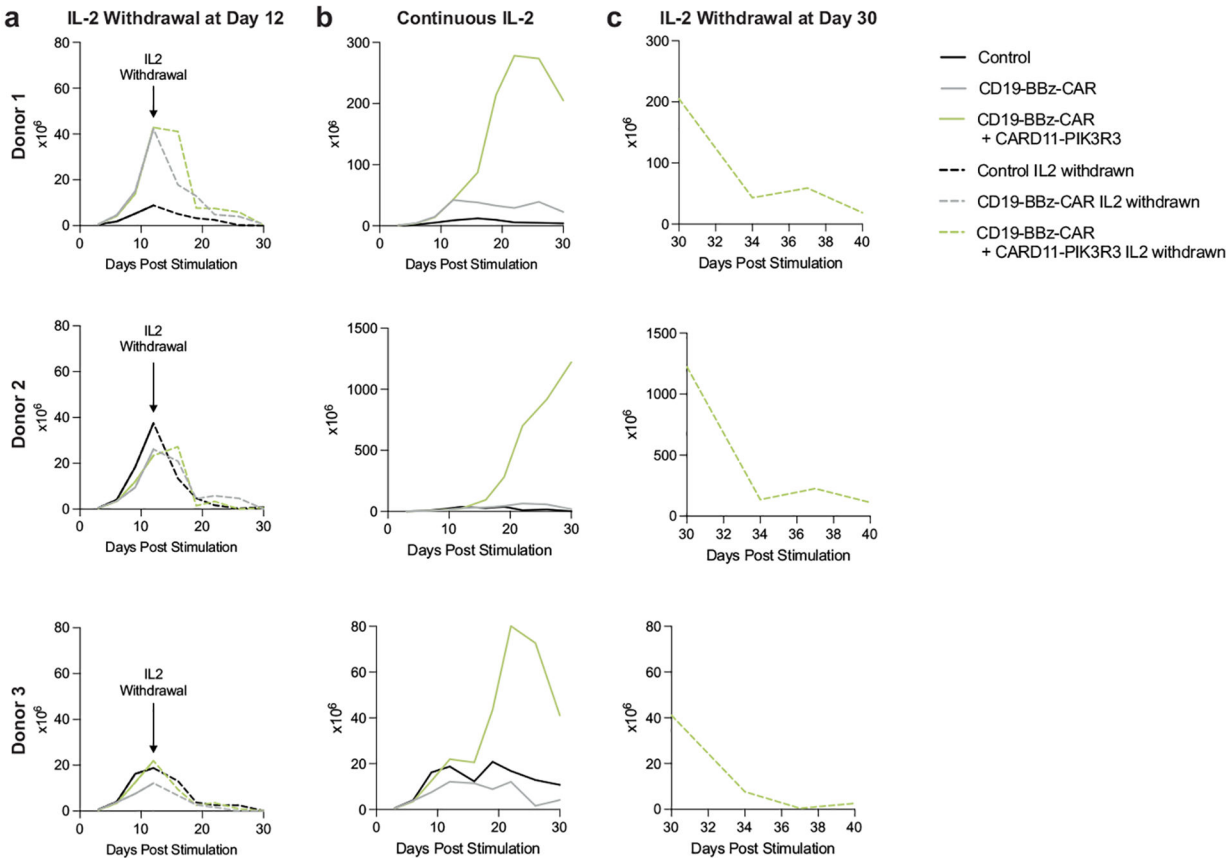

Extended Data Fig. 4 |. In Vitro Expansion of CD19-BBz-CAR T cells with and without CARD11-PIK3R3.

(a,b) CAR or CAR + CARD11-PIK3R3 were sorted for purity, then expanded with IL-2 for 12 days. On Day 12, cultures were split, reseeding each group without IL-2 **(a)** and with IL-2 **(b)**. Cells were counted and split from day 12 to day 30. **(c)** On Day 30, CD19-BBz-CAR + CARD11-PIK3R3 T cells that were cultured with IL-2 were reseeded without IL-2 and counted and split for an additional 10 days.

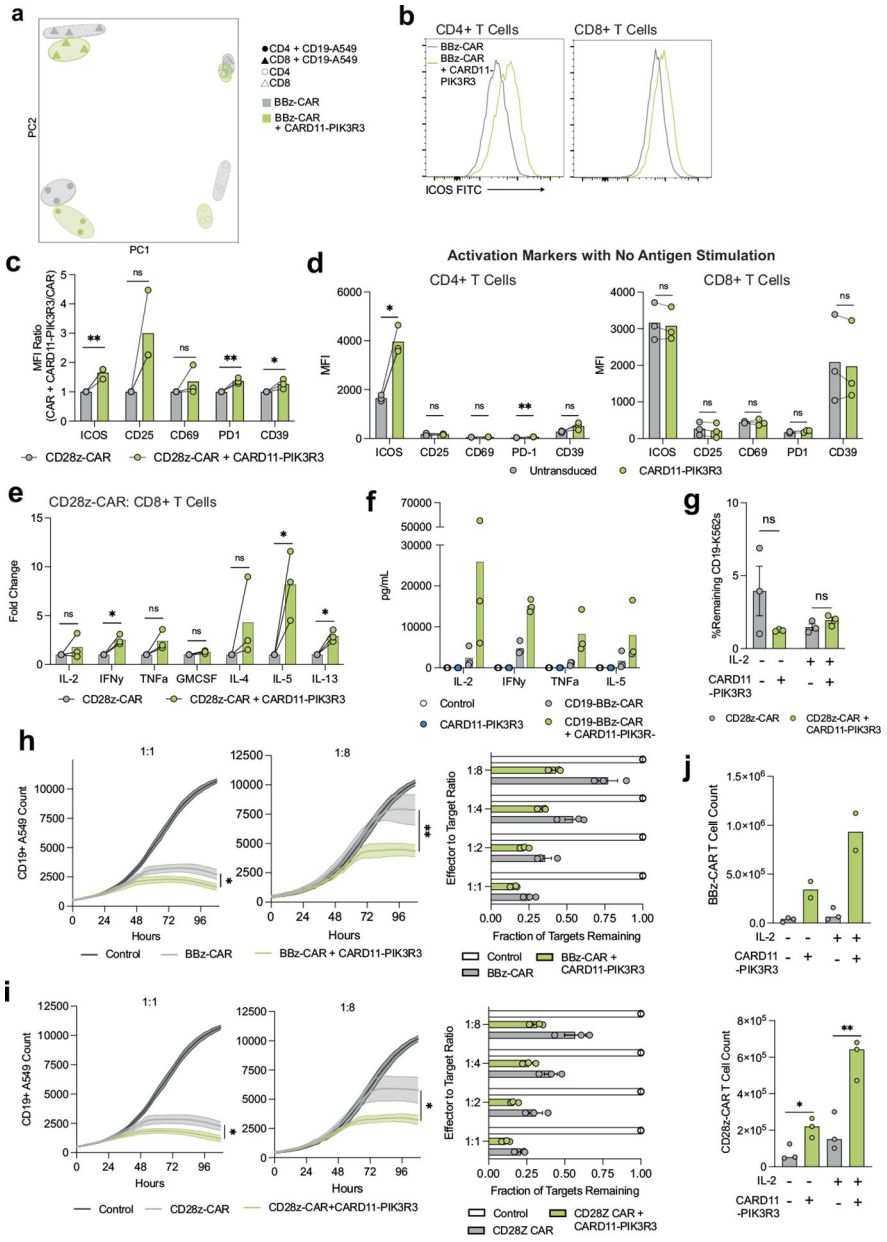

Extended Data Fig. 5 |. In vitro analysis of CARD11-PIK3R3 expressing T cells.

(**a**) Principal component analysis of transcriptomes of human BBz-CAR T cells. (**b**) Representative histogram of ICOS expression on CD19-BBz-CAR T cells 24 h after co-culture with CD19-K562s. (**c**) Activation markers expressed on CD8+ CD19–28z-CAR T cells after 24 h co-cultured with CD19-K562s. Ratio of MFI (CAR + CARD11-PIK3R3/ CAR) shown. P values determined by two-tailed unpaired T test. (**d**) Activation markers expressed on untransduced and CARD11-PIK3R3 CD4+ and CD8 + T cells after 24 h co-cultured with CD19-K562s. P values determined by two-tailed ratio paired T test with Holm-Sidak correction for multiple comparisons. (**e**) Cytokine secretion of CD8 + CD19− CD28z-CAR T cells 48 h post 1:1 co-culture with CD19-K562s. P values determined by two-tailed ratio paired T test, represented as fold change relative to control.

(**f**) Cytokine secretion of control, CARD11-PIK3R3, CD19-BBz-CAR and CD19-BBz-CAR + CARD11-PIK3R3 CD8 + T cells 48 h post 1:1 co-culture with CD19-K562s. (**g**) Bar graph summarizing CD19-K562 population percentages after 14-day co-culture of CD19-CD28z-CAR T cells with and without CARD11-PIK3R3, and supplemental IL-2. P values determined by multiple paired T test followed by Bonferroni correction. (**h-i**) Cell counts of CD19-A549 mKate2+ targets co-cultured with CD8+ (**h**) CD19-BBz-CAR T cells or (**i**) CD19-CD28z-CAR T cells over 108 h period. Bar graph indicates target cell counts at hour 108, standardized to control. P values calculated by one-way ANOVA followed by Tukey's multiple comparison test, performed on cell count at 108 h. (**j**) Cell counts of CD8 + CD19-BBz-CAR T cells or CD19-CD28z-CAR T cells on Day 13 after two stimulations with CD19-K562 targets (n = 2 or 3). P values determined by two-tailed unpaired T test. (**a**,**c-j**) Each data point indicates an independent donor (n = 3), with the exception of j (n = 2 or 3). ns indicates not significant, * indicates P value < 0.05, ** indicates P value < 0.01.

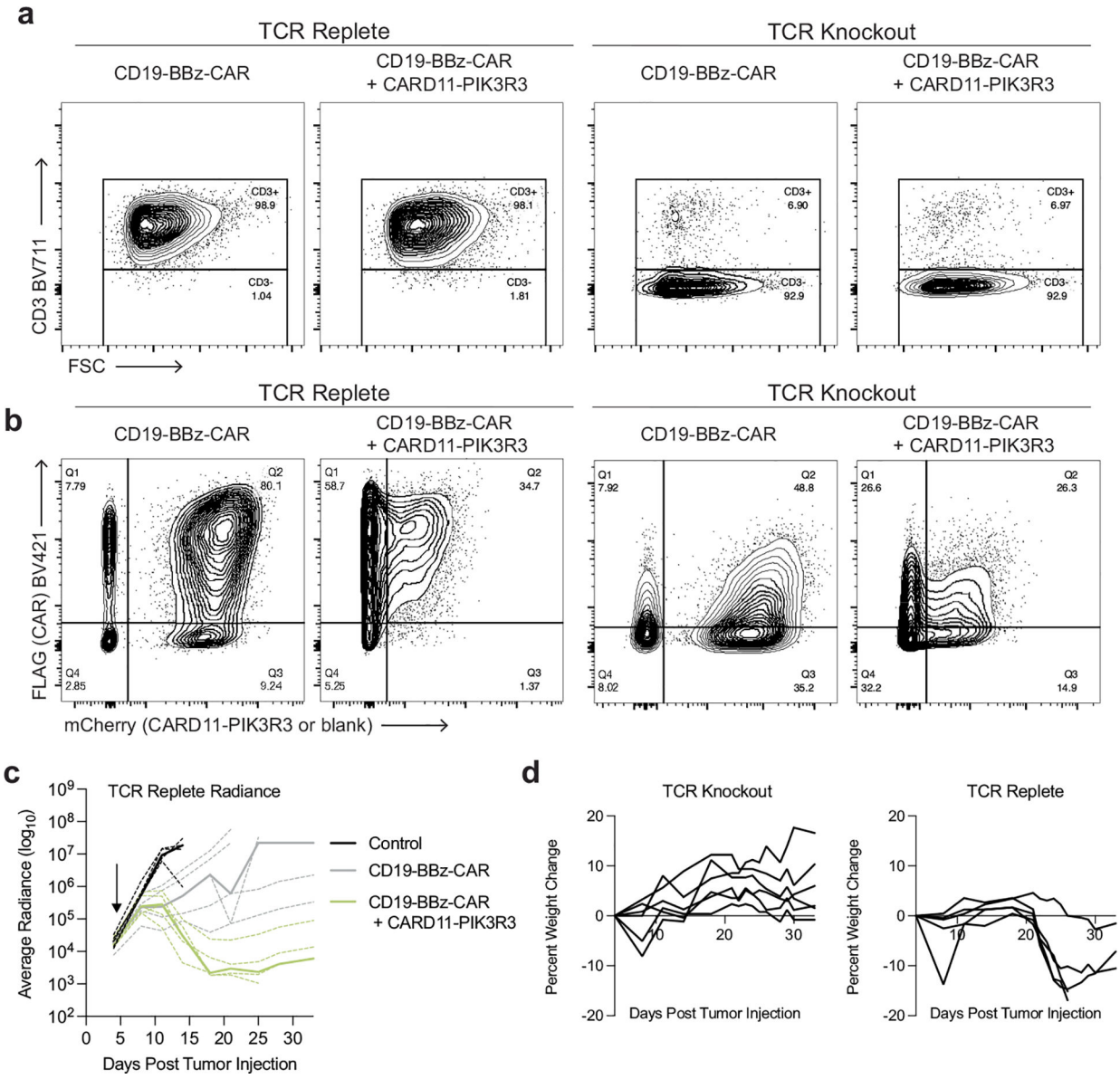

Extended Data Fig. 6 |. Weight loss of CD19-BBz-CAR + CARD11-PIK3R3 treated animals ameliorated with TCR Knockout.

(**a**) Flow cytometry plots indicating CD3 expression of TCR replete or TCR knockout groups after electroporation with TRAC targeted RNPs. (**b**) Flow cytometry plots indicating CAR (FLAG) and CARD11-PIK3R3 or control blank construct (mCherry) expression in human CD3 + T cells. (**c**) Radiance of Nalm6-Luc-GFP tumor bearing animals treated with control (n = 5), CD19-BBz-CAR (n = 5), CD19-BBz-CAR + CARD11-PIK3R3 (n = 5) TCR replete T cells dosed at 1e6 CAR + T cells, control cells dosed equivalent to highest total T cell dose in other treatment groups. Dotted lines indicate individual mice, bold line indicates median. Arrow indicates date T cells were injected. (**d**) Percent weight change from baseline of TCR Knockout or TCR replete CD19-BBz-CAR + CARD11-PIK3R3 treated Nalm6 bearing animals.

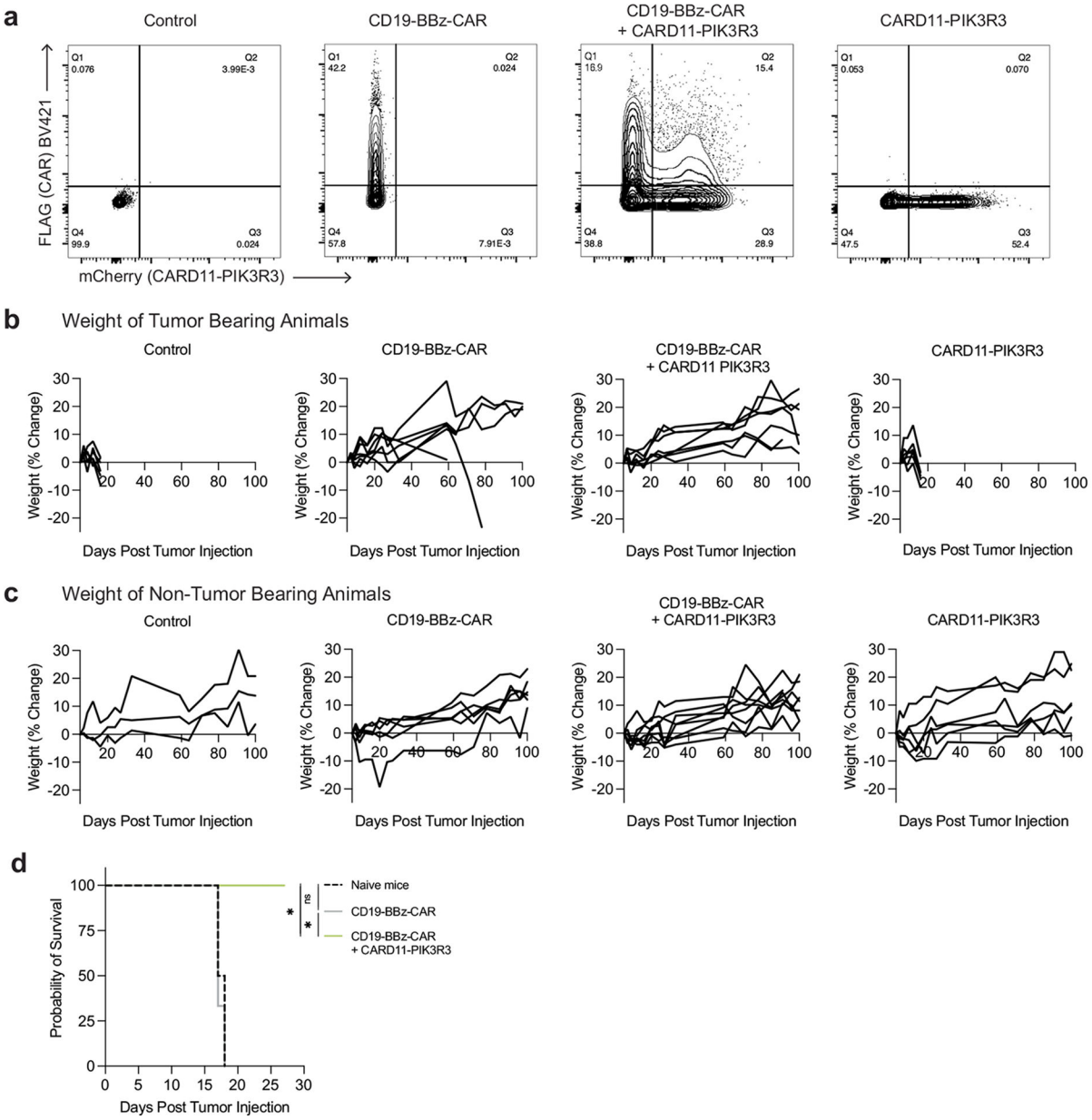

Extended Data Fig. 7 |. CD19-BBz-CAR + CARD11-PIK3R3 is well tolerated and effective at high doses.

(**a**) Flow cytometry plots indicating CAR (FLAG) and CARD11-PIK3R3 (mCherry) expression in human CD3 + T cells. (**b-c**) Percent weight change from baseline of (**b**) tumor bearing or (**c**) non-tumor bearing animals treated with control, CD19-BBz-CAR, CD19-BBz-CAR + CARD11-PIK3R3 or CARD11-PIK3R3 (**d**) Survival analysis of Fig. 4b surviving CD19-BBz-CAR (n = 3), CD19-BBz-CAR + CARD11-PIK3R3 (n = 4) animals or naïve mice (n = 4) rechallenged with 5e5 Nalm6-Luc-GFP tumors. P values determined by Log-rank Mantel-Cox followed by Bonferroni correction. ** indicates P value < 0.01.

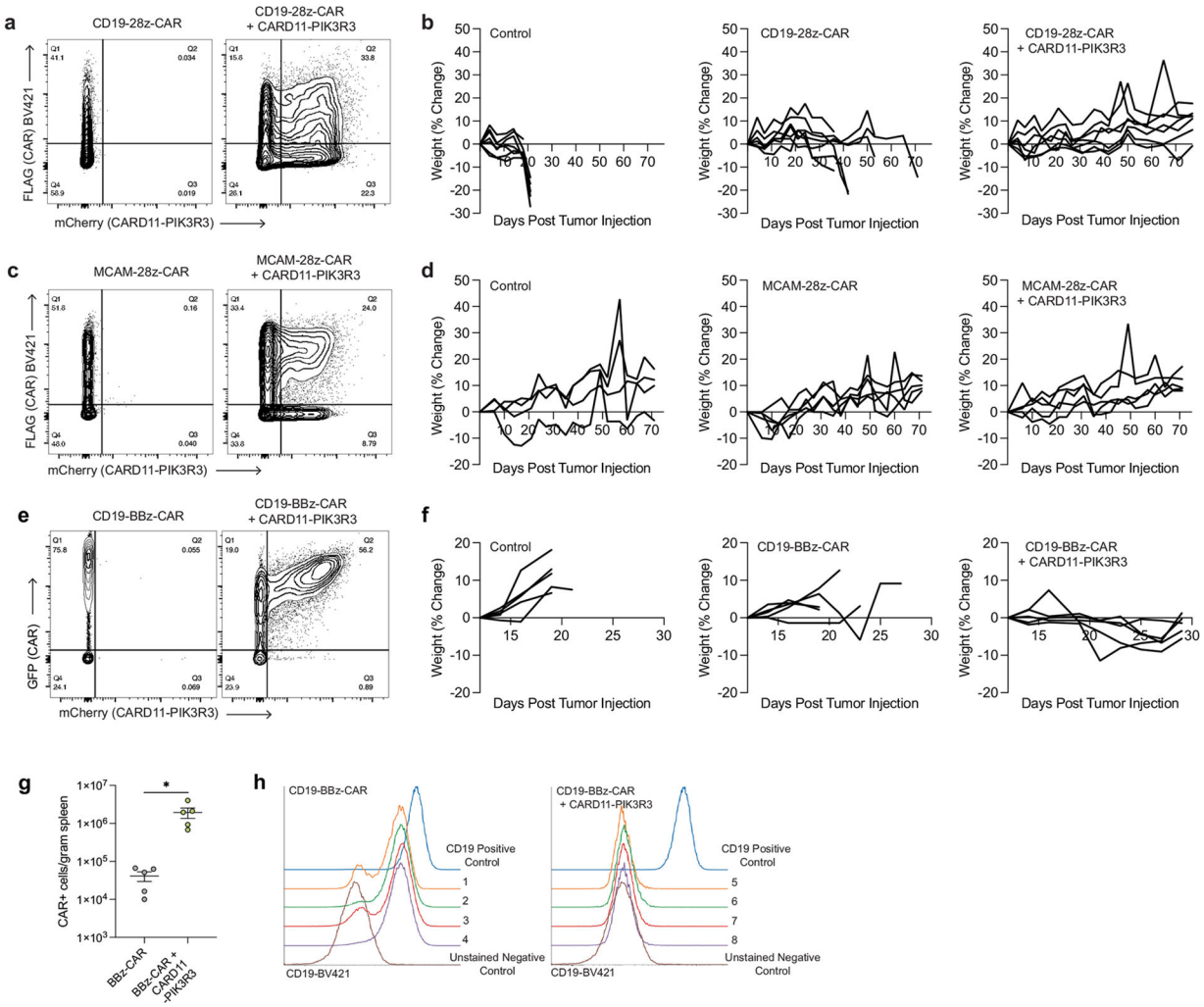

Extended Data Fig. 8 |. In vivo analysis of CARD11-PIK3R3 expressing CAR T cells.

(**a,c**) Flow cytometry plots indicating FLAG (CAR) and mCherry (CARD11-PIK3R3) expression in human CD3 + T cells. **(b)** Percent weight change from baseline of control, CD19-CD28z-CAR or BBz-CAR + CARD11-PIK3R3 treated Nalm6 tumor bearing animals. **(d)** Percent weight change from baseline of control, MCAM-CD28z-CAR or MCAM-CD28z-CAR + CARD11-PIK3R3 treated M28 tumor bearing animals. (**e**) Flow cytometry plots indicating GFP (CAR) and CARD11-PIK3R3 (mCherry) expression in mouse OT-I T cells. (**f**) Percent weight change from baseline of control, CD19-BBz-CAR or CD19-BBz-CAR + CARD11-PIK3R3 treated hCD19-B16 tumor bearing animals. (**g**) Accumulation of CD19-BBz-CAR T cells in spleen of hCD19-B16 tumor bearing animals 5 days post adoptive cell transfer. Each data point indicates one mouse (n = 5), mean + s.e.m. depicted. P values determined using two-tailed unpaired t test. (**h**) Histograms indicating human CD19 ligand expression on hCD19-B16 tumors, CD19-BBz-CAR or CD19-BBz-CAR + CARD11-PIK3R3 treated that had reached euthanasia endpoint, compared to known CD19 positive B16 tumor sample. * indicates P value < 0.05.

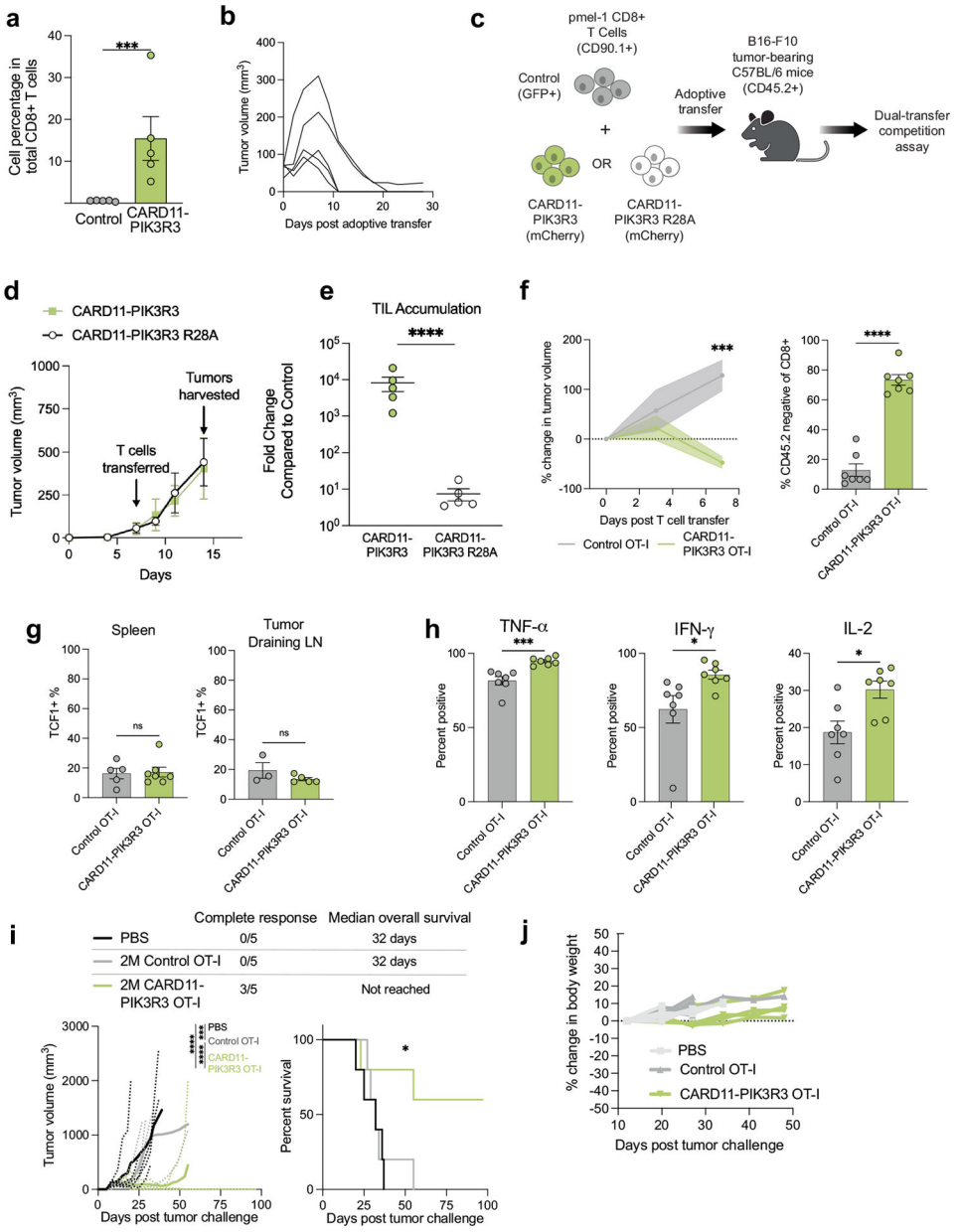

Extended Data Fig. 9 |. In vivo analysis of CARD11-PIK3R3 expressing OT-I T cells.

(**a**) Cell percentage in total CD8 + T cells of control or CARD11-PIK3R3 OT-I T cells in dual transfer experiment (n = 5). P values determined by two-tailed unpaired T test. The images of the mouse and the cells were created with BioRender.com and adapted as required. (**b**) Tumor growth curve for mice bearing B16-OVA tumors treated with 1×10^6 OT-I T cells (10% CARD11-PIK3R3 positive). (**c**) Schematic of competition experiments with pmel-1 CD8 T cells. (**d**) Tumor growth curves of mice described in (c) (n = 5). (**e**) Fold-enrichment in the tumor of wild-type CARD11-PIK3R3 or CARD11-PIK3R3 (p.R28A) expressing pmel-1 CD8 T cells compared to vector control 7 days after adoptive transfer (n = 5). Mean + s.e.m. depicted. All P values determined by two-tailed ratio paired T test. (**f**) Percent change in tumor volume and proportion of transferred cells in control

OT-I (n = 8) and CARD11-PIK3R3 OT-I (n = 9) mice bearing B16-OVA subcutaneous tumors. Each data point indicates one mouse, mean + s.e.m. depicted. (**g**) Frequency of TCF-1 + OT-I cells in spleen (control OT-1 n = 5, CARD11-PIK3R3 OT-1 n = 7) and tumor draining lymph node (LN) (control OT-1 n = 3, CARD11-PIK3R3 OT-1 n = 5) of mice bearing B16-OVA subcutaneous tumors. P values determined by two-tailed unpaired T test. (**h**) Ex vivo cytokine production with PMA/Ionomycin stimulation of control OT-I (n = 7) or CARD11-PIK3R3 OT-I (n = 7) TILs 7 days post T cell transfer. P values determined by two-tailed unpaired T test. (**i**) Tumor volume and survival analysis in B16-OVA melanoma bearing mice treated with PBS (n = 5), control OT-I cells (2×10^6) (n = 5), or CARD11-PIK3R3 OT-I cells (2×10^6) (n = 5) day 12 after tumor inoculation. Complete response was defined as an absence of a detectable tumor. P values determined by one-way ANOVA followed by Tukey's multiple comparisons test (tumor volume) or Log-rank Mantel-Cox (survival). (**j**) Percent change in body weight in PBS, control OT-I, or CARD11-PIK3R3 OT-I treated, B16-OVA tumor bearing mice. Each data point indicates one mouse, mean + s.e.m. depicted. ns indicates not significant, *** indicates P values < 0.001, **** indicates P value < 0.0001.

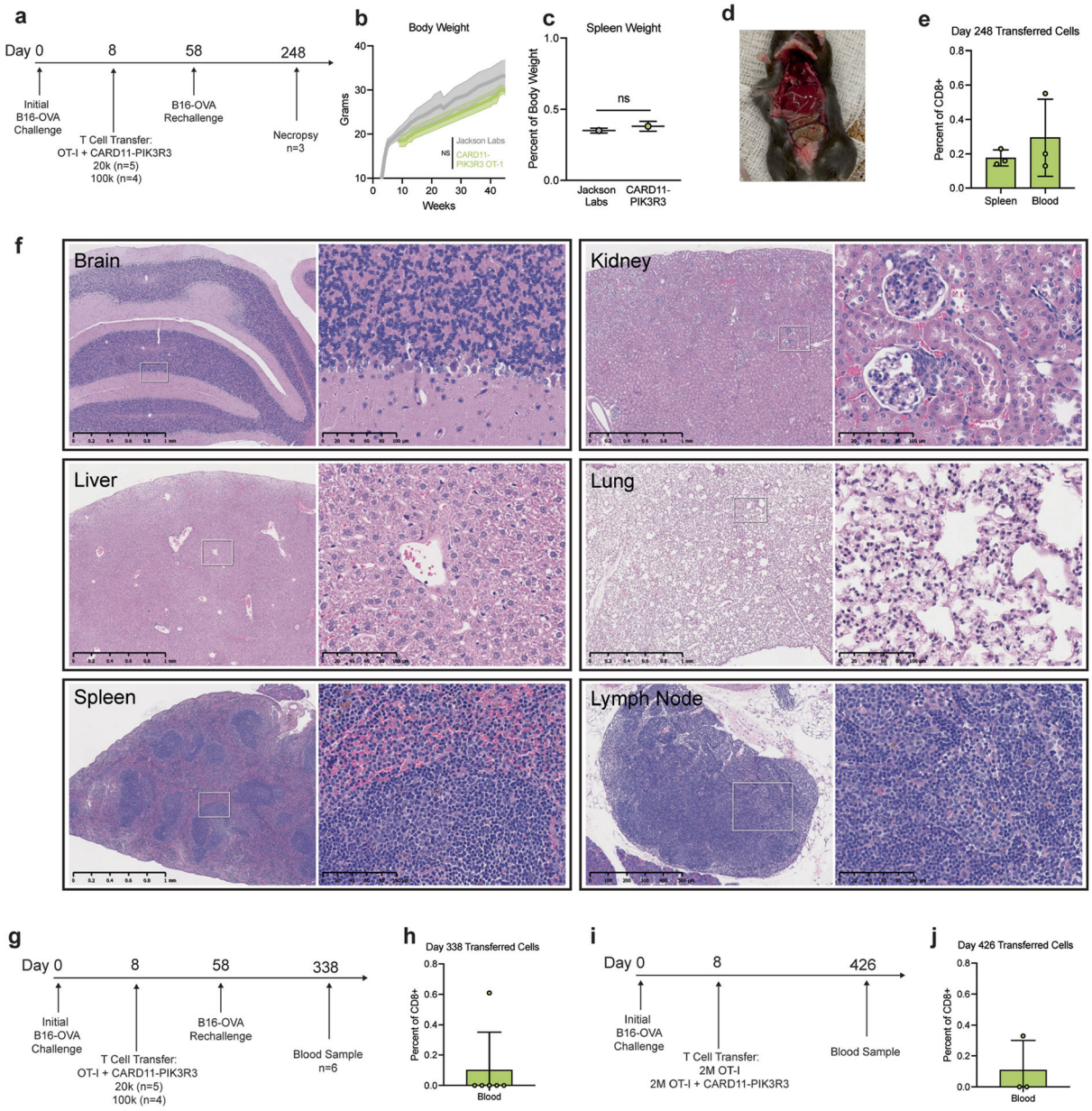

Extended Data Fig. 10 |. Long-term evaluation of B6 mice treated with CARD11-PIK3R3 expressing OT-I T cells.

(**a**) Mice that cleared B16-F10-OVA from Fig. 5e were monitored for up to 240 days after adoptive T cell transfer. Necropsies were performed in as outlined in this schematic. (**b**) Body weights of all CARD11-PIK3R3 infused mice from Fig. 5e and Extended Data Fig. 9i were measured weekly and compared to expected weight curves published by The Jackson Laboratory Research Institute. P value determined by two-way ANOVA. (**c**) Spleen weight for three animals that underwent necropsy on day 240 post adoptive transfer. This was calculated as percent of body weight and compared to expected spleen weight published by The Jackson Laboratory Research Institute. P value determined by two-tailed unpaired T test. (**d**) Necropsy of one representative animal. None of the three animals had gross pathology. (**e**) Percentage of CD8 T cells in spleen and blood that express CARD11-PIK3R3

240 days post adoptive transfer. (**f**) Representative hematoxylin and eosinstained tissue sections from select organs where nodal or extranodal lymphomas can occur. Animals were subject to full-body necropsies (n = 3). Tissues did not show evidence of nuclear atypia, changes in cellular architecture, or presence of neoplastic disease. Representative images at low (left) and high (right) -power magnification are shown with size bars. White box reflects the site of high-magnification image. (**g,i**) Schematic of blood sampling of mice presented in Fig. 5e 330 days after adoptive transfer (**g**) or of 2e6 OT-I CARD11-PIK3R3 treated mice presented in Extended Data Fig. 9i 418 days after adoptive transfer (**i**). (**h,j**) Percentage of CD8 T cells in blood that express CARD11-PIK3R3 in the two cohorts described in Fig. 5e or Extended Data Fig. 9i. Each data point indicates one mouse, mean + s.e.m. depicted.

Supplementary Material

Refer to Web version on PubMed Central for supplementary material.

Acknowledgements

We thank the Northwestern University Flow Cytometry Core, the University of California, San Francisco Flow Cytometry Core, the Northwestern University Research Computing Services, the Northwestern University Skin Biology and Disease Resource-Based Center and Admera Health for their contributions; and J. Eyquem for providing the Nalm6-Luc-expressing cell line. The indicated graphics in Figs. 1a and 5a and Extended Data Fig. 9a were created with BioRender.com and adapted as required. J.D. was supported by NIH NCI grants F30 CA265107 and T32 CA009560. J.G. was supported by NIH NCI grant F31 CA260790. J.C. was supported by NIH grant 1DP2AI136599-01, the Bakewell Foundation and the Mark Foundation Emerging Leader Award. K.T.R. was supported by the Parker Institute for Cancer Immunotherapy, the NIH-NCI Cancer Moonshot Immuno-Oncology Translational Network Center Grant (U54 CA244438), the UCSF Helen Diller Family Comprehensive Cancer Center and the NIH Director's New Innovator Award (DP2 CA239143).

Data availability

Sequencing reads are deposited in the NCBI Sequence Read Archive (BioProject ID PRJNA1029944). All other data are available in the main text or the Supplementary Information. Source data are provided with this paper.

References

1. Hou AJ, Chen LC & Chen YY Navigating CAR-T cells through the solid-tumour microenvironment. Nat. Rev. Drug Discov 20, 531–550 (2021). [PubMed: 33972771]
2. Wang L et al. Genomic profiling of Sézary syndrome identifies alterations of key T cell signaling and differentiation genes. Nat. Genet 47, 1426–1434 (2015). [PubMed: 26551670]
3. Rafiq S, Hackett CS & Brentjens RJ Engineering strategies to overcome the current roadblocks in CAR T cell therapy. Nat. Rev. Clin. Oncol 17, 147–167 (2020). [PubMed: 31848460]
4. Larson RC & Maus MV Recent advances and discoveries in the mechanisms and functions of CAR T cells. Nat. Rev. Cancer 21, 145–161 (2021). [PubMed: 33483715]
5. Mustjoki S & Young NS Somatic mutations in "benign" disease. N. Engl. J. Med 384, 2039–2052 (2021). [PubMed: 34042390]
6. Walker S et al. Identification of a gain-of-function STAT3 mutation (p.Y640F) in lymphocytic variant hypereosinophilic syndrome. Blood 127, 948–951 (2016). [PubMed: 26702067]
7. Park J et al. Genomic analysis of 220 CTCLs identifies a novel recurrent gain-of-function alteration in RLTPR (p.Q575E). Blood 130, 1430–1440 (2017). [PubMed: 28694326]
8. Park J et al. Integrated genomic analyses of cutaneous T-cell lymphomas reveal the molecular bases for disease heterogeneity. Blood 138, 1225–1236 (2021). [PubMed: 34115827]

9. Daniels J et al. Cellular origins and genetic landscape of cutaneous gamma delta T cell lymphomas. Nat. Commun 11, 1806–1806 (2020). [PubMed: 32286303]
10. Stadtmauer Edward A et al. CRISPR-engineered T cells in patients with refractory cancer. Science 367, eaba7365 (2020). [PubMed: 32029687]
11. Fraietta JA et al. Disruption of TET2 promotes the therapeutic efficacy of CD19-targeted T cells. Nature 558, 307–312 (2018). [PubMed: 29849141]
12. Prinzing B et al. Deleting DNMT3A in CAR T cells prevents exhaustion and enhances antitumor activity. Sci. Transl. Med 13, eabh0272. [PubMed: 34788079]
13. Martinez GJ et al. The transcription factor NFAT promotes exhaustion of activated $CD8^+$ T cells. Immunity 42, 265–278 (2015). [PubMed: 25680272]
14. Schmitz R et al. Burkitt lymphoma pathogenesis and therapeutic targets from structural and functional genomics. Nature 490, 116–120 (2012). [PubMed: 22885699]
15. Liu Y et al. The genomic landscape of pediatric and young adult T-lineage acute lymphoblastic leukemia. Nat. Genet 49, 1211–1218 (2017). [PubMed: 28671688]
16. Lynn RC et al. c-Jun overexpression in CAR T cells induces exhaustion resistance. Nature 576, 293–300 (2019). [PubMed: 31802004]
17. Legut M et al. A genome-scale screen for synthetic drivers of T cell proliferation. Nature 603, 728–735 (2022). [PubMed: 35296855]
18. Kahan SM et al. Intrinsic IL-2 production by effector CD8 T cells affects IL-2 signaling and promotes fate decisions, stemness, and protection. Sci. Immunol 7, eabl6322 (2022). [PubMed: 35148200]
19. Ruland J & Hartjes L CARD-BCL-10-MALT1 signalling in protective and pathological immunity. Nat. Rev. Immunol 19, 118–134 (2019). [PubMed: 30467369]
20. Jattani RP, Tritapoe JM & Pomerantz JL Intramolecular interactions and regulation of cofactor binding by the four repressive elements in the caspase recruitment domain-containing protein 11 (CARD11) inhibitory domain. J. Biol. Chem 291, 8338–8348 (2016). [PubMed: 26884334]
21. Burke JE Structural basis for regulation of phosphoinositide kinases and their involvement in human disease. Mol. Cell 71, 653–673 (2018). [PubMed: 30193094]
22. Kutzner K et al. Phosphorylation of serine-893 in CARD11 suppresses the formation and activity of the CARD11-BCL10-MALT1 complex in T and B cells. Sci. Signal 15, eabk3083. [PubMed: 35230873]
23. Li S, Yang X, Shao J & Shen Y Structural insights into the assembly of CARMA1 and BCL10. PLoS ONE 7, e42775 (2012). [PubMed: 22880103]
24. Grossmann A et al. Phospho-tyrosine dependent protein-protein interaction network. Mol. Syst. Biol 11, 794 (2015). [PubMed: 25814554]
25. Fan X, Quezada SA, Sepulveda MA, Sharma P & Allison JP Engagement of the ICOS pathway markedly enhances efficacy of CTLA-4 blockade in cancer immunotherapy. J. Exp. Med 211, 715–725 (2014). [PubMed: 24687957]
26. Massarelli E et al. High OX-40 expression in the tumor immune infiltrate is a favorable prognostic factor of overall survival in non-small cell lung cancer. J. Immunother. Cancer 7, 351 (2019). [PubMed: 31843013]
27. Bardet M et al. The T-cell fingerprint of MALT1 paracaspase revealed by selective inhibition. Immunol. Cell Biol 96, 81–99 (2018). [PubMed: 29359407]
28. Jiang T, Zhou C & Ren S Role of IL-2 in cancer immunotherapy. Oncoimmunology 5, e1163462 (2016). [PubMed: 27471638]
29. Guedan S et al. Enhancing CAR T cell persistence through ICOS and 4–1BB costimulation. JCI Insight 10.1172/jci.insight.96976 (2018).
30. King MA et al. Human peripheral blood leucocyte non-obese diabetic-severe combined immunodeficiency interleukin-2 receptor gamma chain gene mouse model of xenogeneic graft-versus-host-like disease and the role of host major histocompatibility complex. Clin. Exp. Immunol 157, 104–118 (2009). [PubMed: 19659776]

31. Bidlingmaier S et al. Identification of MCAM/CD146 as the target antigen of a human monoclonal antibody that recognizes both epithelioid and sarcomatoid types of mesothelioma. Cancer Res. 69, 1570–1577 (2009). [PubMed: 19221091]
32. Li Q-X, Feuer G, Ouyang X & An X Experimental animal modeling for immuno-oncology. Pharmacol. Ther 173, 34–46 (2017). [PubMed: 28167217]
33. Kalbasi A et al. Potentiating adoptive cell therapy using synthetic IL-9 receptors. Nature 607, 360–365 (2022). [PubMed: 35676488]
34. Overwijk WW & Restifo NP B16 as a mouse model for human melanoma. Curr. Protoc. Immunol 10.1002/0471142735.im2001s39 (2001).
35. Wei J et al. Targeting REGNASE-1 programs long-lived effector T cells for cancer therapy. Nature 576, 471–476 (2019). [PubMed: 31827283]
36. Leidner R et al. Neoantigen T-cell receptor gene therapy in pancreatic cancer. New Engl. J. Med 386, 2112–2119 (2022). [PubMed: 35648703]
37. Zhao H et al. Genome-wide fitness gene identification reveals Roquin as a potent suppressor of CD8 T cell expansion and anti-tumor immunity. Cell Rep. 37, 110083 (2021). [PubMed: 34879274]
38. FDA investigating serious risk of T-cell malignancy following BCMA-directed or CD19-directed autologous chimeric antigen receptor (CAR) T cell immunotherapies. FDA https://www.fda.gov/vaccines-blood-biologics/safety-availability-biologics/fda-investigating-serious-risk-t-cell-malignancy-following-bcma-directed-or-cd19-directed-autologous (28 November 2023).
39. Cappell KM & Kochenderfer JN Long-term outcomes following CAR T cell therapy: what we know so far. Nat. Rev. Clin. Oncol 20, 359–371 (2023). [PubMed: 37055515]
40. Tward JD, Wendland MM, Shrieve DC, Szabo A & Gaffney DK The risk of secondary malignancies over 30 years after the treatment of non-Hodgkin lymphoma. Cancer 107, 108–115 (2006). [PubMed: 16708354]
41. Chihara D, Dores GM, Flowers CR & Morton LM The bidirectional increased risk of B-cell lymphoma and T-cell lymphoma. Blood 138, 785–789 (2021). [PubMed: 33822002]
42. Harrison SJ et al. CAR^+ T-cell lymphoma post ciltacabtagene autoleucel therapy for relapsed refractory multiple myeloma. Blood 142, 6939 (2023).
43. Bowcock SJ et al. High incidence of therapy-related myelodysplasia and acute leukaemia in general haematology clinic patients treated with fludarabine and cyclophosphamide for indolent lymphoproliferative disorders. Br. J. Haematol 134, 242–243 (2006). [PubMed: 16846486]
44. Zhu I et al. Modular design of synthetic receptors for programmed gene regulation in cell therapies. Cell 185, 1431–1443 (2022). [PubMed: 35427499]
45. Morsut L et al. Engineering customized cell sensing and response behaviors using synthetic notch receptors. Cell 164, 780–791 (2016). [PubMed: 26830878]
46. Roybal KT et al. Precision tumor recognition by T cells with combinatorial antigen-sensing circuits. Cell 164, 770–779 (2016). [PubMed: 26830879]
47. Porter DL, Levine BL, Kalos M, Bagg A & June CH Chimeric antigen receptor–modified T cells in chronic lymphoid leukemia. New Engl. J. Med 365, 725–733 (2011). [PubMed: 21830940]
48. Jutz S et al. Assessment of costimulation and coinhibition in a triple parameter T cell reporter line: simultaneous measurement of NF-κB, NFAT and AP-1. J. Immunol. Methods 430, 10–20 (2016). [PubMed: 26780292]

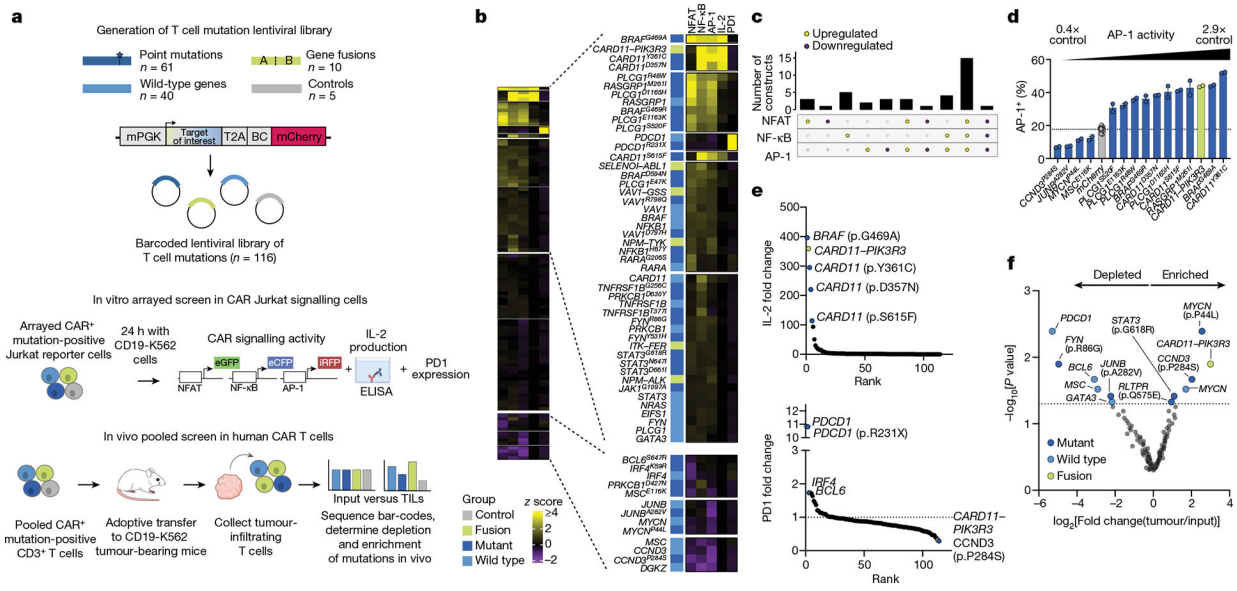

Fig. 1 |. In vitro and in vivo screening identifies T cell mutations that reprogram CAR signalling and functional outputs.

a, A schematic of T cell mutation screening. BC, bar-code. The images of the cells were created with BioRender.com and adapted as required. **b**, A heat map of the reporter activity (*z* score) for the indicated T cell mutation constructs in the BBz-CAR CD19-K562 screen. Clustering was determined using *k*-means. The *z* score indicates the mean *z* score, normalized to mCherry-only controls, of two independent experimental replicates. Select clusters with pronounced effects are highlighted. **c**, An upset plot demonstrating unique signalling outputs of mutations in the BBz-CAR CD19-K562 screen. **d**, A bar graph indicating the percentage of AP-1 positivity in BBz-CAR cells following CD19-K562 stimulation of select mutations. Each point represents an experimental replicate ($n = 2$); mean ± s.e.m. is depicted. **e**, IL-2 and PD1 fold change in the BBz-CAR CD19-K562 screen. The fold change represents the mean of two independent experimental replicates as compared to mCherry controls. **f**, A volcano plot indicating enrichment or depletion in vivo for each construct as determined by MAGeCK. A positive $\log_2$[fold change] indicates an increased persistence in tumours compared to input.

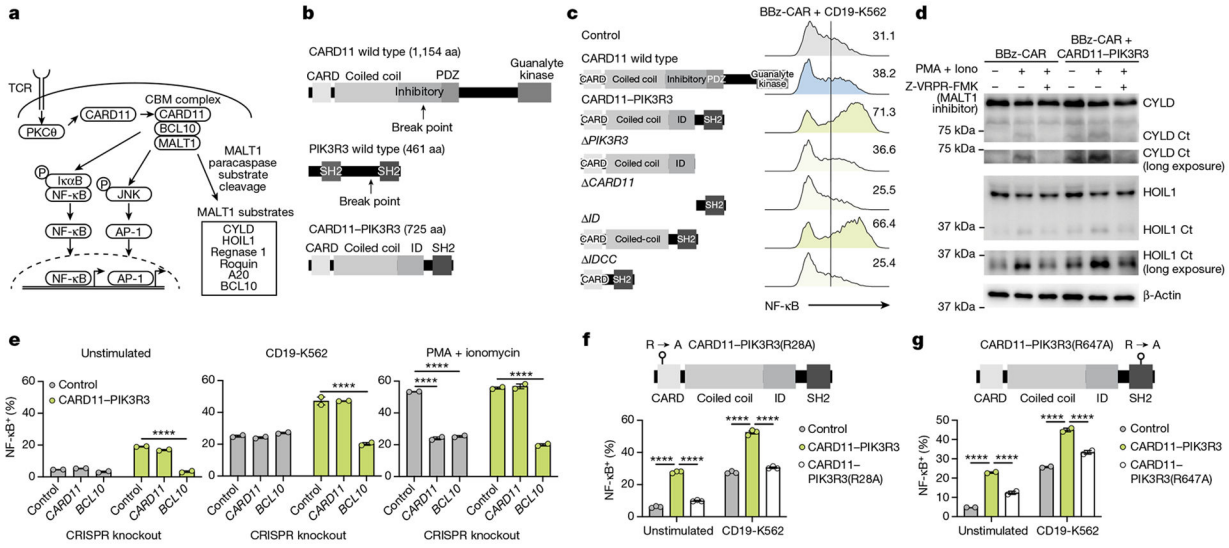

Fig. 2 |. CARD11–PIK3R3 enhances CBM complex signalling.

a, A schematic of CBM signalling in T cells. **b**, Diagrams of CARD11, PIK3R3 and CARD11–PIK3R3. **c**, NF-κB reporter activity of BBz-CAR CARD11–PIK3R3 Jurkat cells co-cultured with CD19-K562 cells. Numbers indicate percent of cells positive. The data are representative of two independent experiments. **d**, MALT1 substrate expression in control or CARD11–PIK3R3-expressing BBz-CAR Jurkat cells. The data are representative of two independent experiments. PMA, phorbol myristate acetate; Iono, ionomycin; Ct, C-terminal cleavage product. **e**, NF-κB reporter activity of control, *CARD11*-knockout or *BCL10*-knockout BBz-CAR Jurkat cells. Each point represents an experimental replicate ($n = 2$); mean ± s.e.m. is depicted. **f**,**g**, Reporter activity of BCL10-binding-deficient ($n = 3$) (**f**) and phospho-tyrosine-binding-deficient ($n = 2$) (**g**) CARD11–PIK3R3. Each data point indicates an experimental replicate; mean ± s.e.m. is depicted. ****$P < 0.0001$, two-way analysis of variance (ANOVA) followed by Dunnett's multiple comparison test.

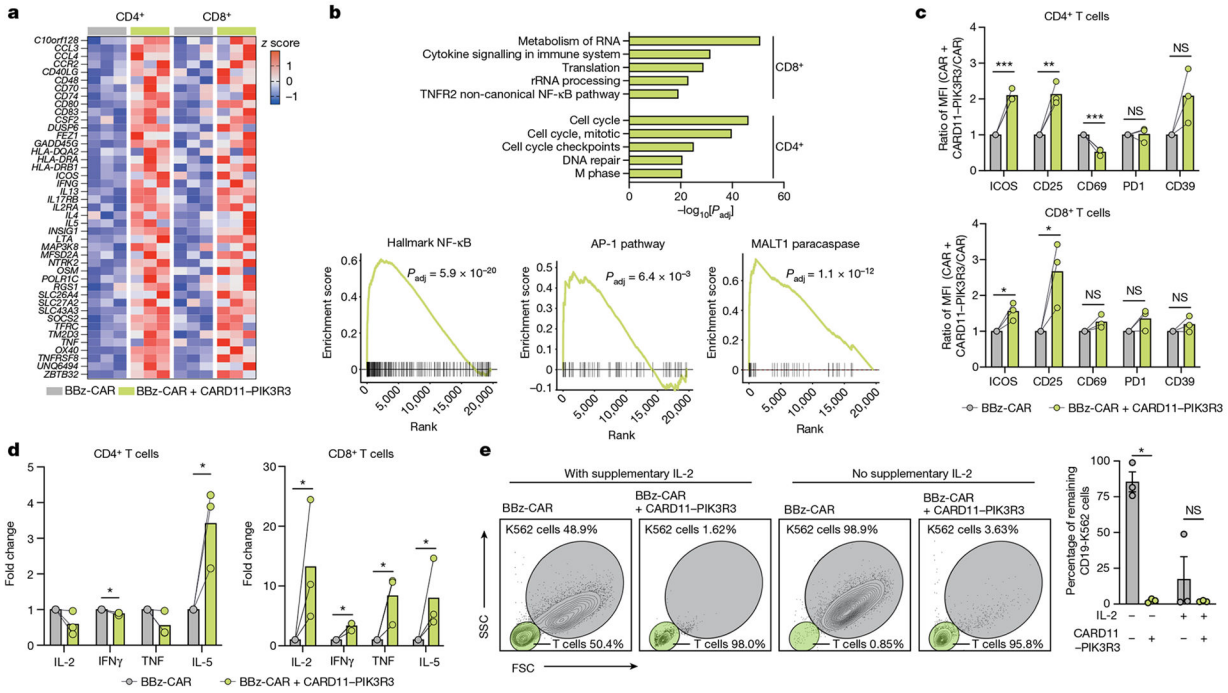

Fig. 3 |. CARD11–PIK3R3 expression leads to signalling, transcriptional and functional enhancements in primary human CD8$^+$ T cells.

a, A heat map of significantly upregulated genes in CARD11–PIK3R3 compared to control BBz-CAR T cells after stimulation with CD19 antigen shared among both CD4$^+$ and CD8$^+$ T cells; each column represents an independent donor. **b**, The top five Reactome pathways enriched in CD4$^+$ and CD8$^+$ T cells (top) and NF-κB, AP-1 and MALT1 gene signature enrichment in CARD11–PIK3R3-expressing CD8$^+$ BBz-CAR T cells after stimulation (bottom) through gene set enrichment analysis. **c**, Activation markers expressed following CD19-K562 stimulation. The *P* values were determined by a two-tailed unpaired *t*-test. MFI, mean fluorescence intensity. **d**, Cytokine secretion following CD19-K562 cell stimulation. The *P* values were determined by a two-tailed ratio paired *t*-test. **e**, Left: flow cytometry plots depicting CD8$^+$ T cell and CD19-K562 populations after 14-day co-culture. Right: a bar graph summarizing population percentages from three independent donors; mean ± s.e.m. is depicted. The *P* values were determined by a multiple paired *t*-test followed by Bonferroni correction. In **c**–**e**, each data point indicates an independent donor ($n = 3$). NS, not significant; $*P < 0.05$, $**P < 0.01$, $***P < 0.001$.

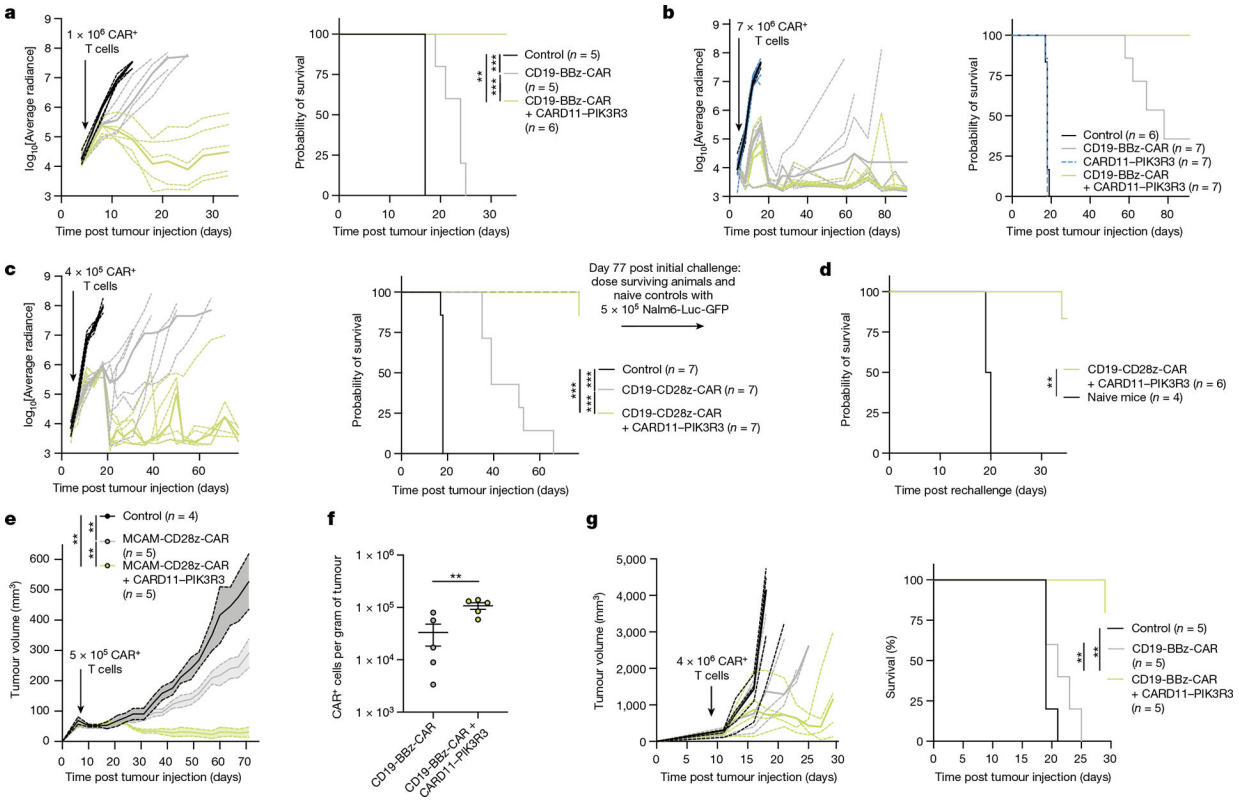

Fig. 4 |. CARD11–PIK3R3 improves the therapeutic efficacy of human and mouse CAR T cells in vivo.

a–**c**, Radiance (left) and survival (right) analysis of Nalm6-Luc-GFP tumour-bearing animals. Radiance was measured using in vivo imaging and used as a proxy for tumour burden. Animals were treated with T cells 5 days post Nalm6 tumour engraftment. In **b**, the treatment of CARD11–PIK3R3 T cells alone was dose adjusted to match the highest CARD11–PIK3R3 dose in other groups. **d**, Survival analysis of surviving CAR + CARD11–PIK3R3 animals or naive mice from **c** rechallenged with Nalm6-Luc-GFP tumours on day 77 post initial tumour injection. **e**, Tumour volumes of M28 tumour-bearing animals treated with T cells 7 days post tumour engraftment. Mean ± s.e.m. is depicted. **f**, Accumulation of CD19-BBz-CAR T cells in hCD19-B16 tumour 5 days post adoptive cell transfer. Each data point indicates an individual mouse ($n = 5$); mean ± s.e.m. is depicted. The P values were determined using two-tailed unpaired t-test. **g**, Tumour volume (left) and survival (right) analysis of hCD19-B16 tumour-bearing animals treated with T cells 9 days post tumour engraftment. The arrows indicate the date of T cell injection. The dashed lines indicate individual mice; the bold lines indicate the median. P values were determined by one-way ANOVA followed by Tukey's multiple comparisons test (tumour volume) or log-rank Mantel–Cox (survival) followed by Bonferroni correction. $^{**}P < 0.01$, $^{***}P < 0.001$.

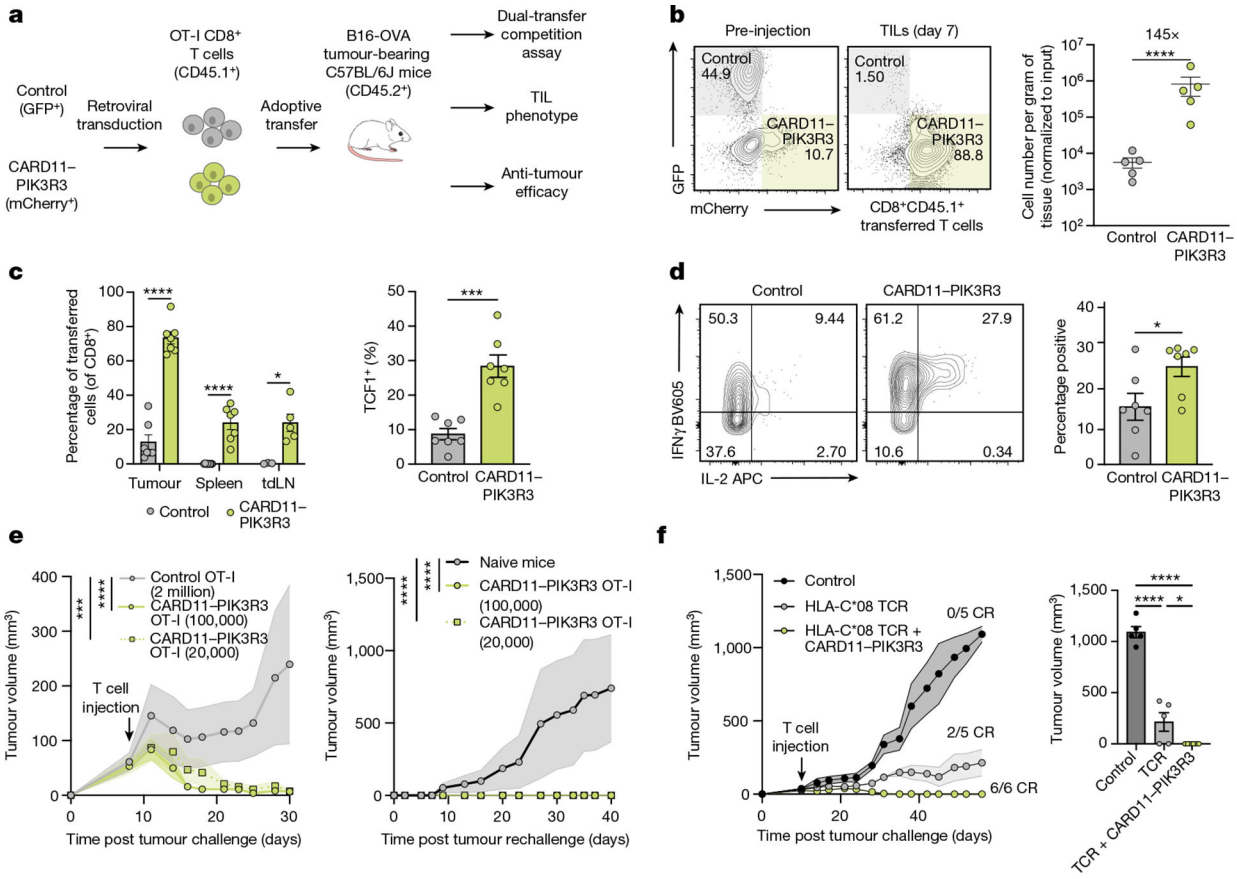

Fig. 5 |. CARD11–PIK3R3 enhances the therapeutic efficacy of mouse and human TCR-transgenic T cells in vivo.

a, Schematic of the syngeneic melanoma model. The images of the cells were created with BioRender.com and adapted as required. **b**, Accumulation of TILs in the competition assay 7 days post T cell transfer ($n = 5$); mean ± s.e.m. is depicted. The P value was determined by two-tailed ratio paired t-test. **c**, Accumulation of TILs in control OT-I-treated ($n = 3$–8) and CARD11–PIK3R3 OT-I-treated ($n = 5$–7) mice (left), and TCF1 expression in tumour-infiltrating OT-I cells ($n = 7$ per group; right); mean ± s.e.m. is depicted. P values were determined by two-tailed unpaired t-test. tdLN, tumour-draining lymph node. **d**, Cytokine production of ex vivo-stimulated OT-I TILs 7 days post T cell transfer ($n = 7$); mean ± s.e.m. of IL-2, TNF and IFNγ triple-positive cells is depicted. P values were determined by two-tailed unpaired t-test. **e**, B16-OVA melanoma tumour volumes in CARD11–PIK3R3 OT-I cells at 100,000 ($n = 4$) or 20,000 ($n = 5$) dose as compared to 2×10^6 OT-I cells ($n = 5$) (left) and rechallenge with B16-OVA melanoma tumours subcutaneously on the contralateral flank (right); mean ± s.e.m. is depicted. P values were determined by one-way ANOVA followed by Tukey's multiple comparisons test. **f**, SNU-1 HLA-C*08:02 gastric cancer xenograft tumour volumes in mice treated with control ($n = 5$), or KRAS(p.G12D)-specific TCR T cells without ($n = 5$) or with ($n = 6$) CARD11–PIK3R3; mean ± s.e.m. is depicted. Complete response (CR) indicates absence of a detectable tumour. P values were determined by one-way ANOVA followed by Tukey's multiple comparisons

test. In **b**–**d**, each data point indicates an individual mouse. *$P < 0.05$, ***$P < 0.001$, ****$P < 0.0001$.